sustainability

MDPI

Article

Updated Predictive Models for Permanent Seismic Displacement of Slopes for Greece and Their Effect on Probabilistic Landslide Hazard Assessment

Dimitris Sotiriadis *, Nikolaos Klimis and Ioannis M. Dokas

Department of Civil Engineering, Democritus University of Thrace, University Campus, 67100 Xanthi, Greece; nklimis@civil.duth.gr (N.K.); idokas@civil.duth.gr (I.M.D.)
* Correspondence: dsotiria@civil.duth.gr

Abstract: Earthquake-triggered landslides have been widely recognized as a catastrophic hazard in mountainous regions. They may lead to direct consequences, such as property losses and casualties, as well as indirect consequences, such as disruption of the operation of lifeline infrastructures and delays in emergency response actions after earthquakes. Regional landslide hazard assessment is a useful tool to identify areas that are vulnerable to earthquake-induced slope instabilities and design prioritization schemes towards more detailed site-specific slope stability analyses. A widely used method to assess the seismic performance of slopes is by calculating the permanent downslope sliding displacement that is expected during ground shaking. Nathan M. Newmark was the first to propose a method to estimate the permanent displacement of a rigid body sliding on an inclined plane in 1965. The expected permanent displacement for a slope using the sliding block method is implemented by either selecting a suite of representative earthquake ground motions and computing the mean and standard deviation of the displacement or by using analytical equations that correlate the permanent displacement with ground motion intensity measures, the slope's yield acceleration and seismological characteristics. Increased interest has been observed in the development of such empirical models using strong motion databases over the last decades. It has been almost a decade since the development of the latest empirical model for the prediction of permanent ground displacement for Greece. Since then, a significant amount of strong motion data have been collected. In the present study, several nonlinear regression-based empirical models are developed for the prediction of the permanent seismic displacements of slopes, including various ground motion intensity measures. Moreover, single-hidden layer Artificial Neural Network (ANN) models are developed to demonstrate their capability of simplifying the construction of empirical models. Finally, implementation of the produced modes based on Probabilistic Landslide Hazard Assessment is undertaken, and their effect on the resulting hazard curves is demonstrated and discussed.

Keywords: seismic slope displacements; strong motion data; landslide hazard assessment; empirical model

check for updates

Citation: Sotiriadis, D.; Klimis, N.; Dokas, I.M. Updated Predictive Models for Permanent Seismic Displacement of Slopes for Greece and Their Effect on Probabilistic Landslide Hazard Assessment. *Sustainability* **2024**, *16*, 2240. https://doi.org/10.3390/su16062240

Academic Editor: Ching-Ying Tsou

Received: 6 February 2024
Revised: 29 February 2024
Accepted: 5 March 2024
Published: 7 March 2024

Copyright: © 2024 by the authors. Licensee MDPI, Basel, Switzerland. This article is an open access article distributed under the terms and conditions of the Creative Commons Attribution (CC BY) license (https://creativecommons.org/licenses/by/4.0/).

1. Introduction

Earthquake-triggered landslides have been widely recognized as a catastrophic hazard in mountainous regions. They may lead to direct consequences, such as property losses and casualties, as well as indirect consequences, such as disruption of the operation of lifeline infrastructures and delays in emergency response actions after earthquakes, which have a serious negative impact on the sustainable development of the society. Regional landslide hazard assessment is a useful tool to identify areas that are vulnerable to earthquake-induced slope instabilities and design prioritization schemes towards more detailed site-specific slope stability analyses.

A widely used method to assess the seismic performance of slopes is by calculating the permanent downslope sliding displacement that is expected during ground shaking.

Newmark (1965) [1] was the first to propose a method to estimate the permanent displacement of a rigid body sliding on an inclined plane. According to the original Newmark's displacement method, the sliding mass is modeled as a rigid block and utilizes two parameters: the critical (or yield) acceleration, a_c, which is defined as the acceleration above which sliding occurs, and the acceleration time-history beneath the sliding mass. This method still forms the basis of many subsequent methods to evaluate the performance of slopes during earthquakes. Subsequent efforts have focused on the inherent weaknesses of Newmark's displacement method, such as the assumption of the rigidity of the sliding mass and its constant yield acceleration [2–4]. The rigid sliding-block assumption is valid for shallow slope failures, which may be found in natural and engineered slopes [5]. However, for deeper sliding surfaces, the deformability and dynamic response of the sliding mass is essential; thus, their consideration in sliding block analyses has been the subject of many research works [2–10].

The expected permanent displacement for a slope using the sliding block method is implemented by either selecting a suite of representative earthquake ground motions and computing the mean and standard deviation of the displacement, or by using analytical equations, which correlate the permanent displacement with ground motion intensity measures (IMs) (e.g., peak ground acceleration PGA, peak ground velocity PGV, Arias Intensity, I_A, etc.), the slope's yield acceleration and seismological characteristics (e.g., earthquake magnitude). Increased interest has been observed in the development of such empirical models using strong motion databases over the last decades. These have been based on classical linear or nonlinear regression [11–19] or, more recently, data-driven artificial neural networks (ANNs) [20–23]. Such models are a basic requirement for the implementation of either deterministic, pseudo-probabilistic or fully probabilistic approaches for the assessment of seismic-induced slope displacements [24]. The latter are suitable for regional landslide assessment as they take into account the variability in both ground motion intensity, the slopes' critical acceleration and slope permanent displacement estimates [25]. Regional landslide assessment is a useful tool to detect areas that are vulnerable to earthquake-induced slope instabilities and help prioritize mitigation measures to ensure the sustainable development of both nature and society.

The latest empirical model for the prediction of seismic-induced slope displacements through the Newmark displacement method for Greece was developed in 2014 [16]. Since then, a significant amount of strong motion data have been compiled [26], and hence, an updated empirical model for Newmark displacements is necessary. Herein, the development of an updated Newmark displacement model for Greece is undertaken, using the most recent strong motion dataset [26]. Multiple nonlinear regression models are developed, having different functional forms and incorporating various strong motion parameters. Furthermore, the capabilities of the Artificial Neural Network technique based on the construction of empirical models for the estimation of slope permanent displacements is highlighted, through an indicative application. Mixed-effects regression analysis of the residuals of the produced models is implemented to obtain the uncertainty model of the empirical expressions. At last, the effect of the selection of the Newmark displacement model on the probabilistic assessment of the seismic-induced slope displacements is emphasized, through example implementation at a site located in the region of East Macedonia and Thrace, Greece.

2. Materials and Methods

2.1. Newmark Displacements and Strong Motion Dataset

The original Newmark method for the estimation of permanent seismic-induced slope displacements models the sliding mass as a rigid block and requires two parameters: the critical (or yield) acceleration, a_c, which is defined as the acceleration that initiates sliding and is affected by the strength properties of the soil material and the slope geometry, together with the acceleration time-history of the rigid plane supporting the sliding mass. A sliding incident begins when the acceleration exceeds a_c and continues until the velocity

of the sliding mass and the rigid plane again coincide. The relative velocity between the rigid mass and the plane beneath is integrated to calculate the relative sliding displacement for each sliding incident, and the sum of the displacements of each incident leads to the cumulative sliding displacement, as shown in Figure 1. More specifically, suppose that a sliding block with critical acceleration equal to a_c = 0.1 g is subjected to the ground acceleration time-history a_g. If, within a time interval t_1–t_2, the critical acceleration is less than a_g, sliding occurs and the acceleration of the block relative to the plane is calculated as follow:

$$a_{rel}(t) = |a_g(t)| - \alpha_c \quad (1)$$

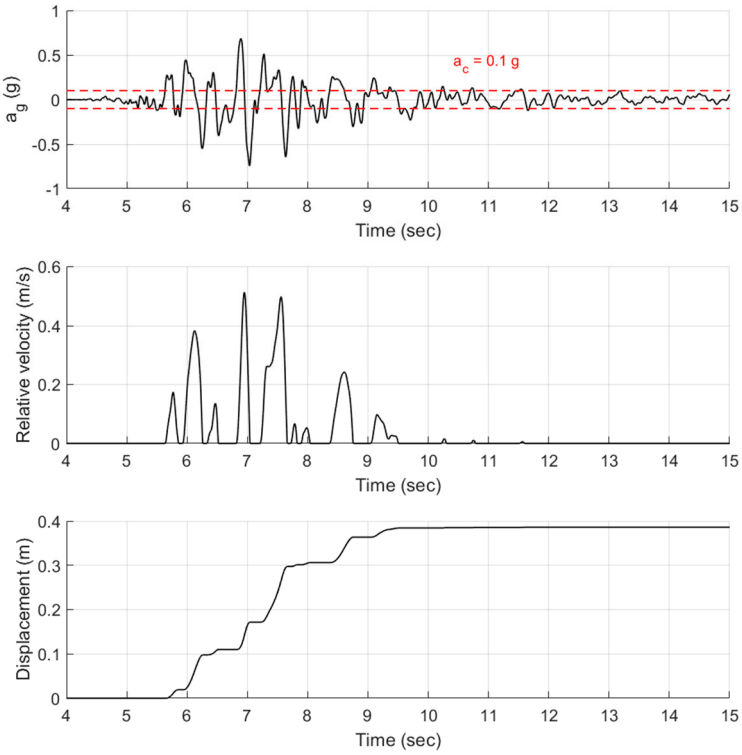


Figure 1. Acceleration time-history, relative velocity time-history and sliding displacement time-history for a rigid sliding mass with a_c = 0.1 g.

The relative movement of the block, within this time interval, can be obtained by integrating the relative acceleration twice, as shown in Equations (2) and (3).

$$v_{rel}(t) = \int_{t1}^{t2} a_{rel}(t)dt \quad (2)$$

$$d_{rel}(t) = \int_{t1}^{t2} v_{rel}(t)dt \quad (3)$$

The most updated strong motion database for shallow earthquakes in Greece has been presented by Margaris et al. (2021) [26]. This database consists of 471 earthquakes that occurred between 1973 and 2015 and produced 2993 recordings resulting from 333 sites. It includes source parameters describing hypocenter locations, moment magnitudes, fault-plane solutions and finite-fault parameters for events with a magnitude larger than 6.0. The average shear-wave velocity of the upper 30 m (V_{S30}) is also provided for all 333 sites. Figure 2 presents the distribution of data with respect to the earthquake magnitude (M_w), the Joyner–Boore distance between the recording station and the rupture (R_{JB}), the focal depth (H), the V_{S30} at the recording station and the peak ground acceleration (PGA). The range of magnitudes lies between $3.8 \leq M_w \leq 7.0$ and distances $\leq$ 300 km. The majority of

the sites exhibits a V_{S30} value ranging between 200 and 600 m/s, while *PGA* values up to 700 cm/s^2 are included. A more detailed presentation of the dataset can be found in [26].

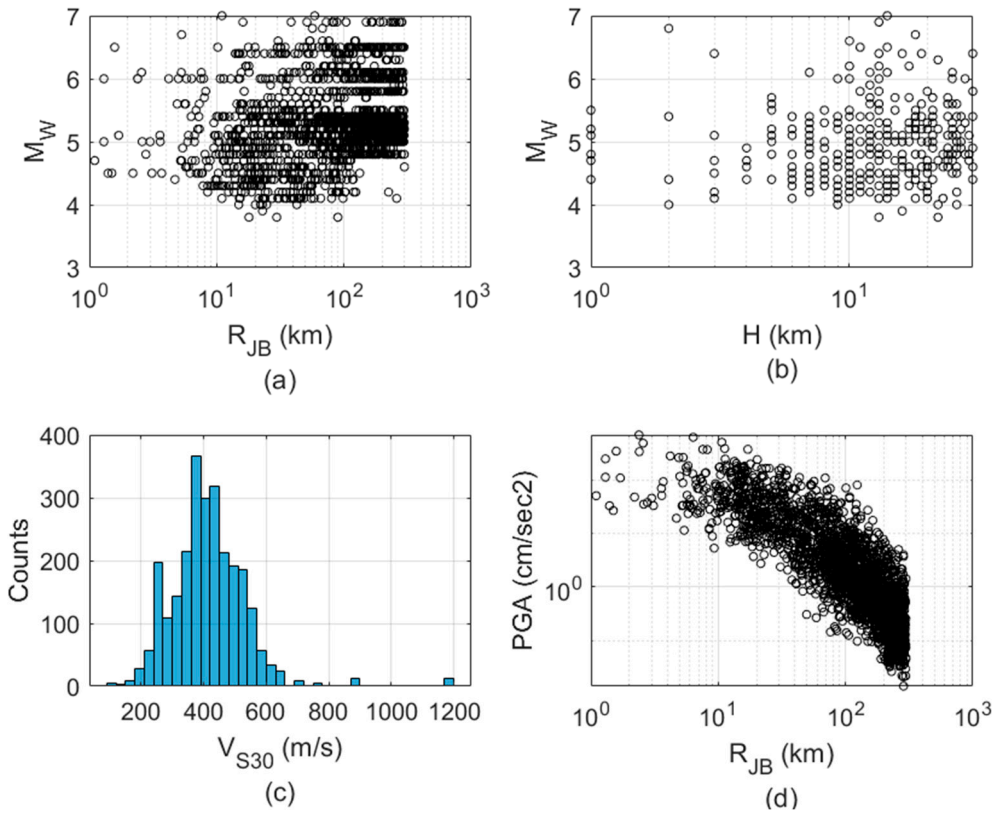


Figure 2. Distribution of ground motion dataset with respect to (**a**) R_{JB} and M_w, (**b**) M_w and H, (**c**) V_{S30} and (**d**) R_{JB} and *PGA*.

In the context of this work, the minimum critical acceleration considered was equal to 0.01 g; therefore, recordings with a *PGA* lower than this threshold were disregarded, as they would lead to zero Newmark displacement. This led to the use of 2772 pairs of recordings of strong motion, for which Newmark displacements and strong motion intensity measures (IMs) were computed for this study. For each recording, the geometrical mean of the two horizontal components was considered as the representative value of the Newmark displacement and the IMs [15]. Several IMs were selected to investigate their impact on the performance of the predictive models based on past experience from the literature [14–16,22,23]. Table 1 presents the IMs considered in this study.

2.2. Empirical Newmark Displacement Predictive Models

In the present study, the development of updated empirical predictive relationships of Newmark displacement for Greece is undertaken. Global Ground Motion Prediction Equations (GMPEs) tend to overestimate the strong motion in Greece [27], and hence, globally calibrated empirical models of Newmark displacement should do so, as well. Hence, the employment of regionally calibrated empirical models is vital for Greece. Towards this, the most updated strong motion database of the Hellenic National Accelerometric Network (HNAN, [26]) is used.

2.2.1. Nonlinear Regression Models

In total, 2772 recordings, consisting of two horizontal components each, were used. Newmark displacement analyses were conducted for 40 critical accelerations ranging between 0.01 g and 0.4 g, and the accumulated Newmark displacements were computed (D_N). This led to the calculation of 110,880 D_N values, from which, the zero values were

omitted. After clearing the dataset, a total of 2468 D_N values and corresponding IMs, earthquake rupture and site parameters were left. Subsequently, nonlinear regression was performed to obtain expressions that estimate D_N as a function of the critical acceleration and several strong motion parameters. The functional form of the investigated expressions was derived from past research existing in the literature. It should be reminded that the geometrical means of D_N and IMs were considered as the dependent and independent variables, respectively. Table 2 presents the models for which the nonlinear regression coefficients were computed, along with their functional form. The last column of Table 2 includes the references that have used the corresponding functional forms. In the functional form of the investigated models, ln refers to the natural logarithm, whereas *log* refers to the logarithm with base 10. Moreover, a_i values are the model coefficients to be determined through nonlinear regression, a_c is the critical acceleration of the slope and the rest of the parameters have been explained in Table 2. Nonlinear regression was performed using MATLAB Simulink R2020b.

Table 1. Intensity measures computed for the strong motion dataset used.

No.	Notation	Name	Definition *
1	*PGA*	Peak Ground Acceleration	$\max\lvert a_g \rvert$
2	*PGV*	Peak Ground Velocity	$\max\lvert v_g \rvert$
3	I_A	Arias Intensity	$\frac{\pi}{2g} \cdot \int_0^{t_{max}} a_g(t)^2 dt$
4	*CAV*	Cumulative Absolute Velocity	$\int_0^{t_{max}} \lvert a_g \rvert dt$
5	a_{rms}	Root Mean Square Acceleration	$\frac{1}{t_d} \cdot \int_0^{t_d} a_g(t)^2 dt t_d = t(95\%I_A) - t(5\%I_A)$
6	I_c	Characteristic Intensity	$I_c = {a_{rms}}^{1.5} \cdot \sqrt{t_d}$
7	*HI*	Housner Intensity	$\int_{0.1}^{2.5} S_{pv} dT$
8	*ASI*	Acceleration Spectrum Intensity	$\int_{0.1}^{0.5} S_{pa} dT$
9	$SD_{5\text{-}95}$	Husid Duration (Time interval between 5% and 95% of I_A)	$t(95\%I_A) - t(5\%I_A)$
10	T_m	Mean Period	$\frac{\sum {C_i}^2 / f_i}{\sum {C_i}^2}, 0.25 \le f_i \le 20$ Hz

* a_g = ground motion acceleration, v_g = ground motion velocity, t = time, g = the acceleration of gravity, S_{pv} = pseudo-velocity spectrum with a 5% damping ratio, S_{pa} = pseudo-acceleration spectrum with a 5% damping ratio, C_i = amplitude of Fourier spectrum, f_i = frequency.

Table 2. Nonlinear regression models considered in this study.

Model	Functional Form	Reference for Functional Form
M1	$\ln D_N = a_0 + a_1(a_c/PGA) + a_2(a_c/PGA)^2 + a_3(a_c/PGA)^3 + a_4 \ln PGA$	[15]
M2	$\ln D_N = a_0 + a_1(a_c/PGA) + a_2(a_c/PGA)^2 + a_3(a_c/PGA)^3 + a_4 \ln PGA + a_5 \ln PGV$	[15]
M3	$\ln D_N = a_0 + a_1(a_c/PGA) + a_2(a_c/PGA)^2 + a_3(a_c/PGA)^3 + a_4 \ln PGA + a_5 \ln PGV + a_6 \ln I_A$	[15]
M4	$\log D_N = a_0 + \log\left[(1 - a_c/PGA)^{a_1} \cdot (\alpha_c/PGA)^{a_2}\right]$	[14]
M5	$\log D_N = a_0 + a_1 \log I_A + a_2 \log a_c$	[14,16]

Table 2. *Cont.*

Model	Functional Form	Reference for Functional Form
M6	$\log D_N = a_0 + a_1 \log I_A + a_2 \log (\alpha_c / PGA)$	[14]
M7	$\ln D_N = a_0 + a_1 \ln(1 - (\alpha_c / PGA) + a_2 \ln (\alpha_c / PGA)$	[11]
M8	$\ln D_N = a_0 + a_1 \ln(1 - (\alpha_c / PGA) + a_2 \ln (\alpha_c / PGA)) + a_3 \ln(PGV)$	[11]
M9	$\ln D_N = a_0 + a_1 \ln (1 - (\alpha_c / PGA)) + a_2 \ln (\alpha_c / PGA)) + a_3 \ln(I_c) + a_4 \ln(PGA)$	[11]
M10	$\ln D_N = a_0 + a_1(\alpha_c / PGA) + a_2(\alpha_c / PGA)^2 + a_3(\alpha_c / PGA)^3 + a_4 \ln PGA + a_5 \ln PGV + a_6 \ln I_A + a_7 \ln CAV + a_8 \ln HI + a_9 \ln ASI + a_{10} \ln I_c + a_{11} \ln SD + a_{12} \ln a_{rms} + a_{13} \ln T_m$	Extension of M3
M11	$\ln D_N = a_0 + a_1(\alpha_c / PGA) + a_2(\alpha_c / PGA)^2 + a_3(\alpha_c / PGA)^3 + a_4 \ln PGA + a_5 \ln PGV + a_6 \ln I_A + a_7 \ln CAV + a_8 \ln HI + a_9 \ln ASI + a_{10} \ln T_m$	Extension of M3
M12	$\ln D_N = a_0 + a_1(\alpha_c / PGA) + a_2(\alpha_c / PGA)^2 + a_3(\alpha_c / PGA)^3 + a_4 \ln PGA + a_5 \ln PGV + a_6 \ln I_c$	Extension of M3
M13	$\log D_N = a_0 + a_1 \log I_c + a_2 \log \alpha_c$	Extension of M5

Models M1–M9 present a functional form and include the strong motion parameters, which are the same with the corresponding reference, shown in the third column of Table 2. However, models M10–M13 are extensions of M3, in that they have a similar functional form and include more or different IMs.

2.2.2. Shallow Artificial Neural Network Models for Newmark Displacement

The functional form, which is adopted to perform the nonlinear regression, highly affects the performance of the predictive models. Such models may have difficulty in capturing nonlinearities in Newmark displacement data, due to the limited number of IMs used and their simple functional form. Alternatively, data-driven artificial neural network (ANN) models can be a flexible solution to describe the complex relationship between response and predictor variables [22]. In this section, shallow ANN models for Newmark displacements were developed to investigate their performance against the more classical regression models. It was intended to develop as much as simple ANN models, which could be easily written in a matrix formulation. Therefore, only one hidden layer of 10 neurons linking the predictor variables to the natural logarithm of D_N was used. The predictor variables were the ones used in models M3 and M12, shown in Table 2. As shown in the results section, those two models were deemed as the most effective in terms of uncertainty and the number of required inputs. Hence, a direct comparison between the capabilities of the nonlinear regression models and simple ANN models can be established. Then, 70% of the data were used to train the ANN models, through the Levenberg–Marquardt backpropagation algorithm [28], whereas the rest of the 30% of the data were used for validation (15%) and testing (15%). The use of logsig and tansig transfer functions was investigated; however, the former provided slightly smaller errors and was preferred. It should be noted that the scope of this study was not to extensively investigate the ANN technique in Newmark displacement prediction, but to preliminary explore its capabilities, using MATLAB Simulink R2020b. Figure 3 presents the architecture of the ANN models considered in this study.

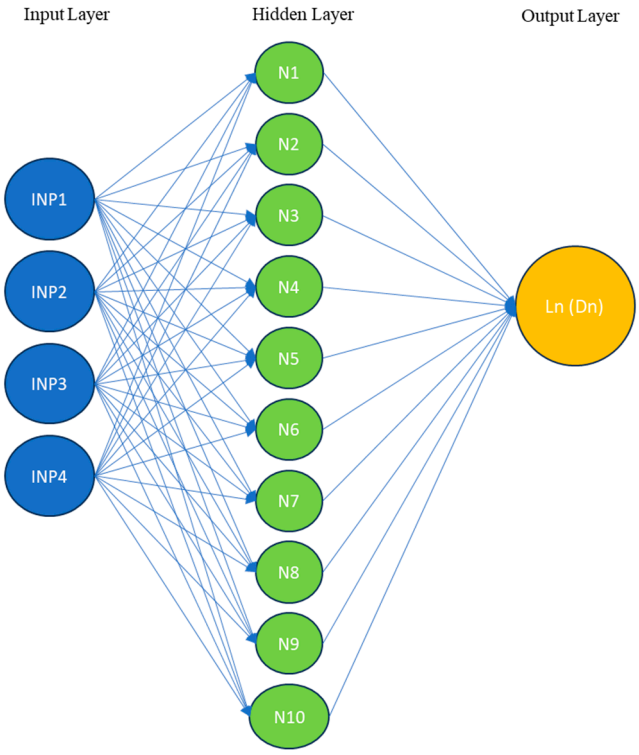


Figure 3. Architecture of the ANN models considered in this study.

2.2.3. Mixed-Effects Regression Based on the Residuals of Selected Models

In this section, the uncertainty of selected nonlinear regression models is calculated using the mixed effects regression based on their residuals. The residuals (R) between the actual Newmark displacements (D_N) and the predicted Newmark displacement (D_{Npr}) based on the regression models are defined in the natural logarithm according to Equation (1). Likewise, with classical Ground Motion Predictive Equations (GMPEs), the mixed-effects analysis aims to produce the aleatory variability model, which describes the between-event and within-event variability of an empirical model [27]. In Equation (1), the indexes i and j denote a seismic event and a recording station, respectively. The second term on the right hand of Equation (1) indicates the mean estimate of the nonlinear regression model, as a function of the considered IMs and the critical acceleration.

$$R_{ij} = \ln D_N - \mu_{\ln DNpr}(IMs, \alpha_c) \quad (4)$$

The mixed effects analysis, proposed by Abrahamson and Youngs (1992) [29], is implemented, so that the residuals are distinguished in between- and within-event residuals, according to Equation (2). In Equation (2), B is the overall bias of the residuals, whereas η_i and ε_{ij} are the between-event and within-event residuals, respectively. The latter residuals (η_i and ε_{ij}) are normally distributed with zero mean values and a standard deviation equal to τ and φ, respectively. Then, the total standard deviation (σ) of each model is computed, based on Equation (3).

$$R_{ij} = B + \eta_i + \varepsilon_{ij} \quad (5)$$

$$\sigma = \sqrt{\tau^2 + \varphi^2} \quad (6)$$

2.3. Probabilistic Landslide Hazard Assessment

The implementation of the Newmark displacement (D_N) models to the probabilistic assessment of landslide hazard is described in this section, to demonstrate the effect of each Newmark displacement model on the sliding displacement hazard curve. The aim is to investigate how the mean annual rate of exceedance of various levels of D_N (λ_{DN}) is

affected when different predictive models, which use various accuracy levels of ground motion description, are incorporated.

The framework for the probabilistic assessment of earthquake-induced sliding displacements presented by [25] is followed herein. According to this, when D_N can be represented by a single ground motion IM, the mean annual rate of exceedance for a displacement level x is defined as follows:

$$\lambda_{DN}(x) = \sum_i P\left[D_N > x | IM_i\right] \cdot P[IM_i] \tag{7}$$

In Equation (4), $P\left[D_N > x \,|\, IM_i\right]$ is the probability that the displacement level x is exceeded provided that the ground motion level is equal to IM_i, and $P\left[IM_i\right]$ is the annual probability of occurrence of IM_i. The former term is derived from the D_N predictive model, whereas the latter is derived from the ground motion hazard curve, which has been calculated through probabilistic seismic hazard assessment (PSHA), as described in [25]. If D_N is a function of two IMs ($IM1$ and $IM2$), then λ_{DN} is given by Equation (5).

$$\lambda_{DN}(x) = \sum_i \sum_j P\left[D_N > x | IM1_i,\ IM2_j\right] \cdot P[IM1_i,\ IM2_j] \tag{8}$$

In Equation (5), $P\left[D_N > x | IM1_i,\ IM2_j\right]$ is the probability of D_N larger than x given the joint occurrence of $IM1_i$ and $IM2_j$, and $P[IM1_i,\ IM2_i]$ is the joint annual probability of the occurrence of $IM1_i$ and $IM2_j$. Normally, the latter term is provided by a vector PSHA analysis. However, herein, the approximation proposed by [25] is followed and is expressed by Equation (6).

$$P\left[IM1_i,\ IM2_j\right] = \left(\sum_l \sum_m P\left[IM2_j \middle| IM1_i, M_l,\ R_m\right] \cdot P[M_l,\ R_m]\right) \cdot P[IM1_i] \tag{9}$$

In Equation (6), $P[IM_i]$ is the probability of the occurrence of $IM1$, $P[M_l,\ R_m]$ is the probability of the occurrence of different earthquake magnitude (M) and source-to-site distance (R) pairs and can be derived via a seismic hazard disaggregation analysis and $P\left[IM2_j \middle| IM1_i, M_l,\ R_m\right]$ is the probability of $IM2$ conditional on $IM1_i$ and the earthquake scenario M_l, R_m. The latter term can be calculated through GMPEs for $IM2$ and $IM1$ along with the correlation coefficient between them, as shown in [30]. Accordingly, if D_N is a function of three IMs ($IM1$, $IM2$, $IM3$), Equations (7) and (8) apply.

$$\lambda_{DN}(x) = \sum_i \sum_j \sum_k P\left[D_N > x | IM1_i,\ IM2_j,\ IM3_k\right] \cdot P[IM1_i,\ IM2_j,\ IM3_k] \tag{10}$$

$$P\left[IM1_i,\ IM2_j, IM3_k\right] = \left(\sum_l \sum_m P\left[IM3_k \middle| IM2_j, IM1_i, M_l,\ R_m\right] \cdot \left[IM2_j \middle| IM1_i, M_l,\ R_m\right] \cdot P[M_l,\ R_m]\right) \cdot P[IM1_i] \tag{11}$$

As an illustrative example, we present here the probabilistic assessment of seismic-induced slope displacements for the cut slopes of a vertical road axis connecting the city of Komotini, located in the region of East Macedonia and Thrace, Greece and the Hellenic-Bulgarian borders. This case has been investigated in [31] with the aim to produce seismic fragility curves for the cut slopes. Representative engineering properties of the local geological formations are given in [31], as well as the geometric features of the slopes. Based on these characteristics, the critical acceleration, a_c, for the cut-slopes varies between 0.05 and 0.3 g, based on the infinite slope model. The PSHA of the whole region of East Macedonia and Thrace, as well as the seismic hazard disaggregation, has been presented in terms of PGA and PGV in [32], whereas the PSHA in terms of I_A was included in [33]. Indicative results of those studies, which are necessary for the probabilistic assessment of seismic-induced slope displacements according to Equations (7)–(11), are shown in Figure 4. Figure 4a presents the seismic hazard curve of the site of interest in terms of I_A, whereas Figure 4b presents the seismic hazard curve in terms of PGA. Furthermore,

Figure 4c presents the seismic hazard disaggregation at the site, in terms of *PGA* for a return period of 465 years.

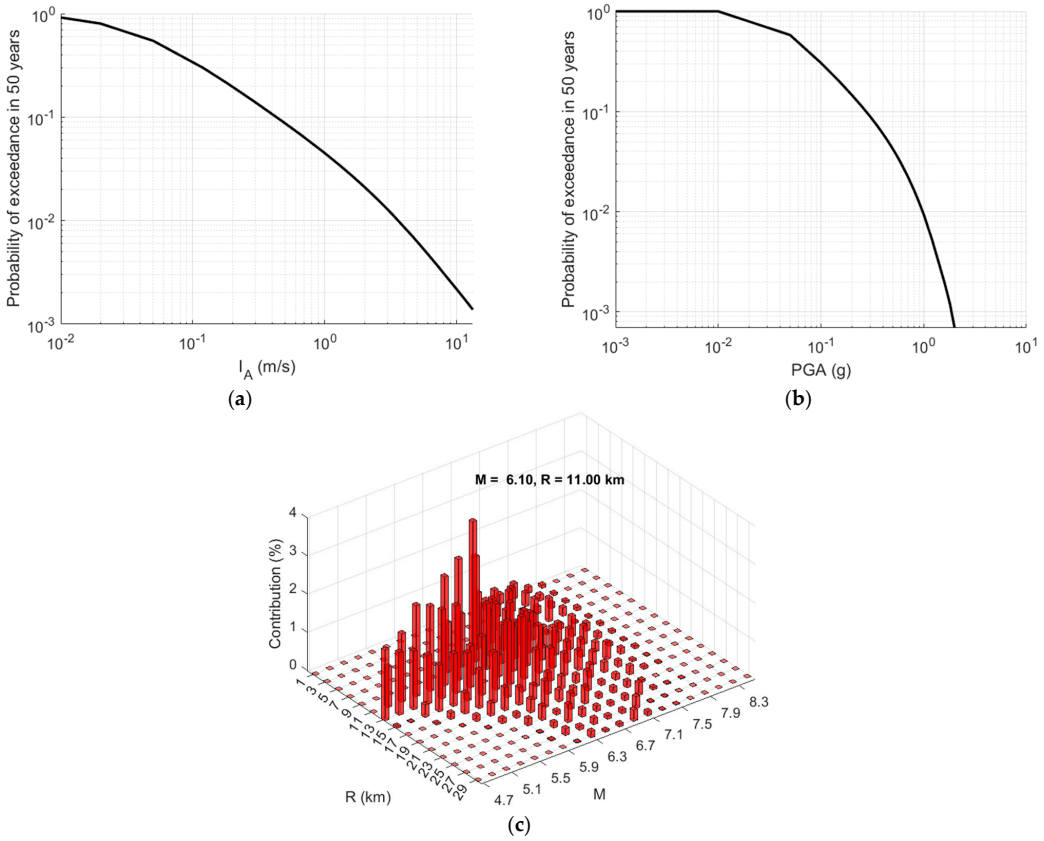


Figure 4. Seismic hazard curve for (**a**) IA and (**b**) PGA and (**c**) disaggregation of seismic hazard in terms of PGA for the site under investigation.

Figure 4 indicates that the *PGA* value corresponding to a return period of 475 years (probability of exceedance equal to 10% in 50 years based on the Poisson distribution), which is the design level for seismic action for ordinary structures, is equal to 0.25 g, whereas the I_A at the same return period is equal to 0.44 m/s. The contribution of various M–R scenarios to the *PGA* level for the return period of 475 years is shown in Figure 4c. The highest contribution originates from small-to-moderate earthquake magnitudes and a source-to-site distance up to 17 km.

3. Results

3.1. Nonlinear Regression Models

Initially, all D_N values larger than zero were included in the nonlinear regression process. However, for almost all investigated models, large overestimations of the Newmark displacements were observed for D_N values smaller than 0.01 cm, as shown in Figure 5. Figure 5 presents the residuals (observed–predicted) in natural logarithm terms, with respect to D_N, for three of the examined models.

After this observation, it was decided to disregard the data with D_N values lower than 0.01 cm. The number of the omitted data was about 300; however, the performance indexes of the examined models were improved by 13% to 40%.

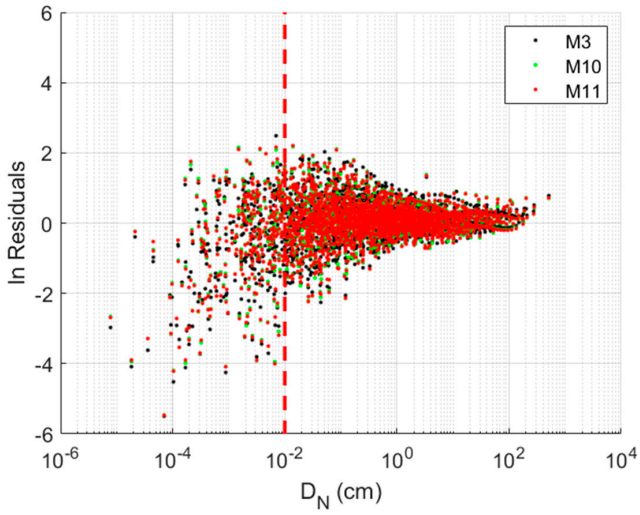


Figure 5. Residuals of ln (DN) with respect to DN for the three examined models. The red dashed line presents the threshold of 0.01 cm.

Table 3 presents the best estimates of the nonlinear regression coefficients (a_i) of the examined models, along with their total standard deviation in natural logarithm terms ($\sigma_{\ln DN}$), the R^2 coefficient, the Akaike's Information Criterion (AIC) and the Bayesian Information Criterion (BIC). The last terms function as performance indexes of the regressed models, with lower $\sigma_{\ln DN}$, AIC and BIC denoting a more accurate model. According to those performance indexes, the most accurate model is M11, which includes eleven coefficients and seven IMs, along with the critical acceleration ratio (a_c/PGA). It should be noted that model M11 behaves even better than model M10, which comes in second place and additionally includes a_{rms}, I_c and SD. The third best-performing model is M12, which is slightly more accurate than M3. M3 originates from the functional form of Saygili and Rathje (2008) [15] and includes three IMs, along with the critical acceleration ratio. M12 is similar to M3, with the only difference being the replacement of I_a with I_c. As models M11 and M10 require too many IMs, models M3 and M12 should be considered optimal choices, as they require only three IMs and the critical acceleration of the slope and they present similar total standard deviations to M11 and M10. Places 5–7 are taken by models needing two IMs to provide estimates of D_N. The best two-IM model is M9, originating from Ambraseys and Menu (1988) [11], and requires PGA and I_c, along with a_c. Model M2, adopted from Saygili and Rathje (2008) [15], presents similar performance indexes to M9 and uses PGV instead of I_c. Regarding the models that require only one IM, M13, which uses I_c and a_c, seems to be the most accurate, followed by M5, which incorporates I_A instead of I_c. From the above, it can be concluded that I_c is probably a better predictor of D_N than I_A.

Figures 6–9 present the residuals (in natural logarithm) of the examined models with respect to the slope's critical acceleration (a_c), the earthquake magnitude (M), the distance between the earthquake rupture and the recording station (R_{JB}) and the Newmark displacements, to detect any possible bias. The red lines plotted along with the residuals indicate their trend with respect to the variable plotted in the horizontal axis. Figure 6 indicates that the residuals of all the examined models but a few exceptions (M4, M6, M7, M8) do not present significant bias with respect to a_c. The plots of Figure 7 denote that models M3 and M9–M13 exhibit no bias with respect to the earthquake magnitude, whereas the rest of them do. The latter are models that incorporate one or two IMs; therefore, information is missing from them to adequately describe the variation in D_N, as was also noted by Saygili and Rathje (2008) [15]. Similar observations with Figure 7 are also made for Figure 8, regarding the bias of the examined models with respect to the site-to-source distance. The inclusion of more than two IMs seems to negate the necessity to include earthquake features, such as the magnitude and the site-to-source distance. Finally,

Figure 9 shows that most of the examined models tend to produce increased residuals with an increasing D_N. Models M3, M10, M11 and M12, however, seem unbiased with respect to D_N.

Table 3. Nonlinear regression coefficients and performance indexes of investigated Newmark displacement models.

Model	M1	M2	M3	M4	M5	M6	M7	M8	M9	M10	M11	M12	M13
a_0	5.276	−2.881	−4.412	−0.806	−5.115	−1.975	−1.857	−2.283	−18.890	−53.424	−0.116	−12.204	−9.4413
a_1	−12.125	−11.578	−11.359	1.404	1.646	0.603	1.404	2.604	2.746	−11.304	−11.299	−11.053	2.2358
a_2	9.678	8.891	8.521	−1.833	−2.222	−2.283	−1.833	−0.962	−1.007	8.477	8.453	7.548	−2.3708
a_3	−6.102	−6.859	−6.952	-	-	-	-	1.078	2.289	−6.995	−6.971	−6.126	-
a_4	1.062	−1.043	−1.607	-	-	-	-	-	−2.330	−1.665	−1.650	−2.199	-
a_5	-	1.845	1.034	-	-	-	-	-	-	0.578	0.583	1.046	-
a_6	-	-	0.799	-	-	-	-	-	-	−6.870	1.532	1.397	-
a_7	-	-	-	-	-	-	-	-	-	−0.688	−0.666	-	-
a_8	-	-	-	-	-	-	-	-	-	−0.655	−0.663	-	-
a_9	-	-	-	-	-	-	-	-	-	0.356	0.356	-	-
a_{10}	-	-	-	-	-	-	-	-	-	5.116	1.256	-	-
a_{11}	-	-	-	-	-	-	-	-	-	5.868	-	-	-
a_{12}	-	-	-	-	-	-	-	-	-	9.165	-	-	-
a_{13}	-	-	-	-	-	-	-	-	-	1.250	-	-	-
$\sigma_{\ln DN}$	1.040	0.628	0.514	1.403	0.908	0.930	1.403	0.741	0.624	0.481	0.481	0.511	0.840
R^2	0.779	0.920	0.946	0.598	0.831	0.823	0.598	0.888	0.920	0.953	0.953	0.947	0.856
AIC	6288.10	4114.31	3249.08	7574.59	5701.53	5801.33	7574.59	4827.37	4088.26	2975.26	2970.79	3224.28	5364.21
BIC	6316.47	4148.36	3288.81	7591.61	5718.55	5818.36	7591.61	4850.07	4116.64	3054.72	3033.21	3264.01	5381.24

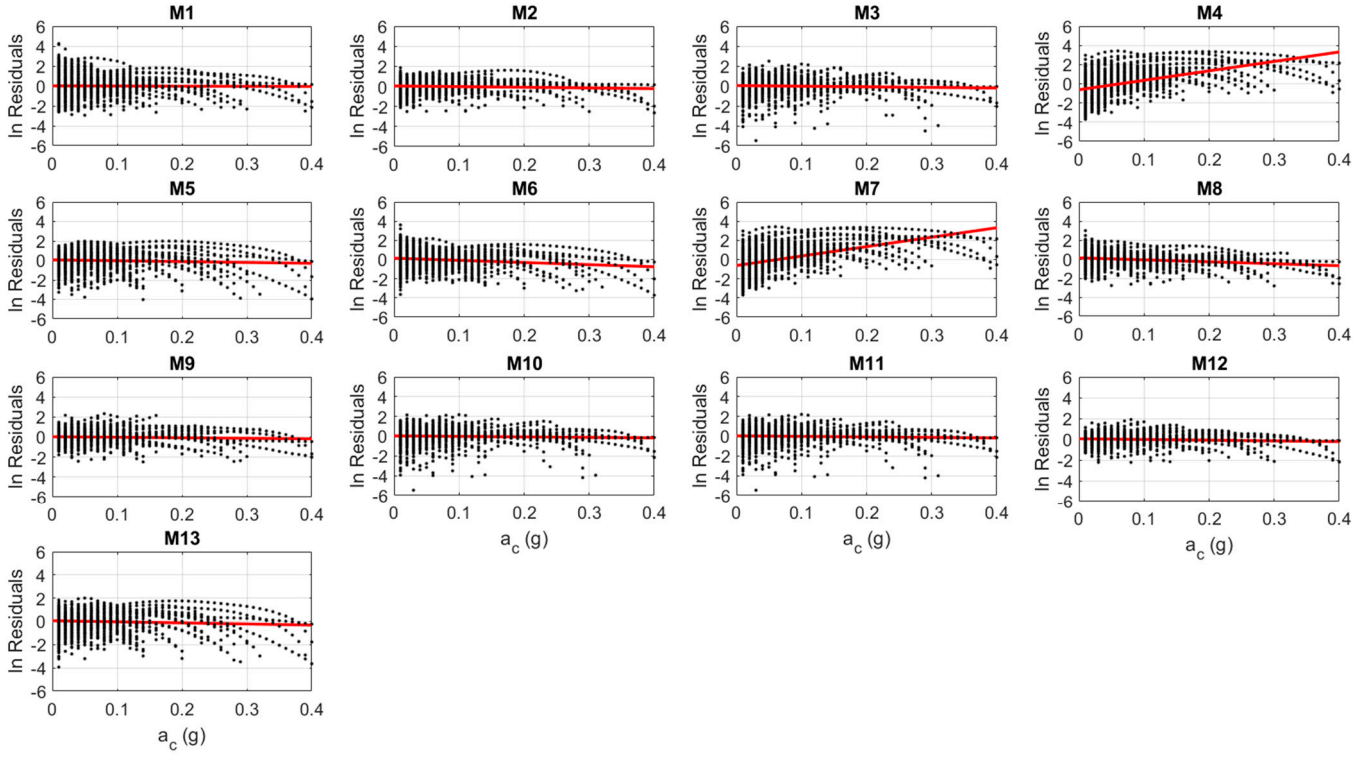


Figure 6. Residuals of nonlinear regression models with respect to the slope's critical acceleration.

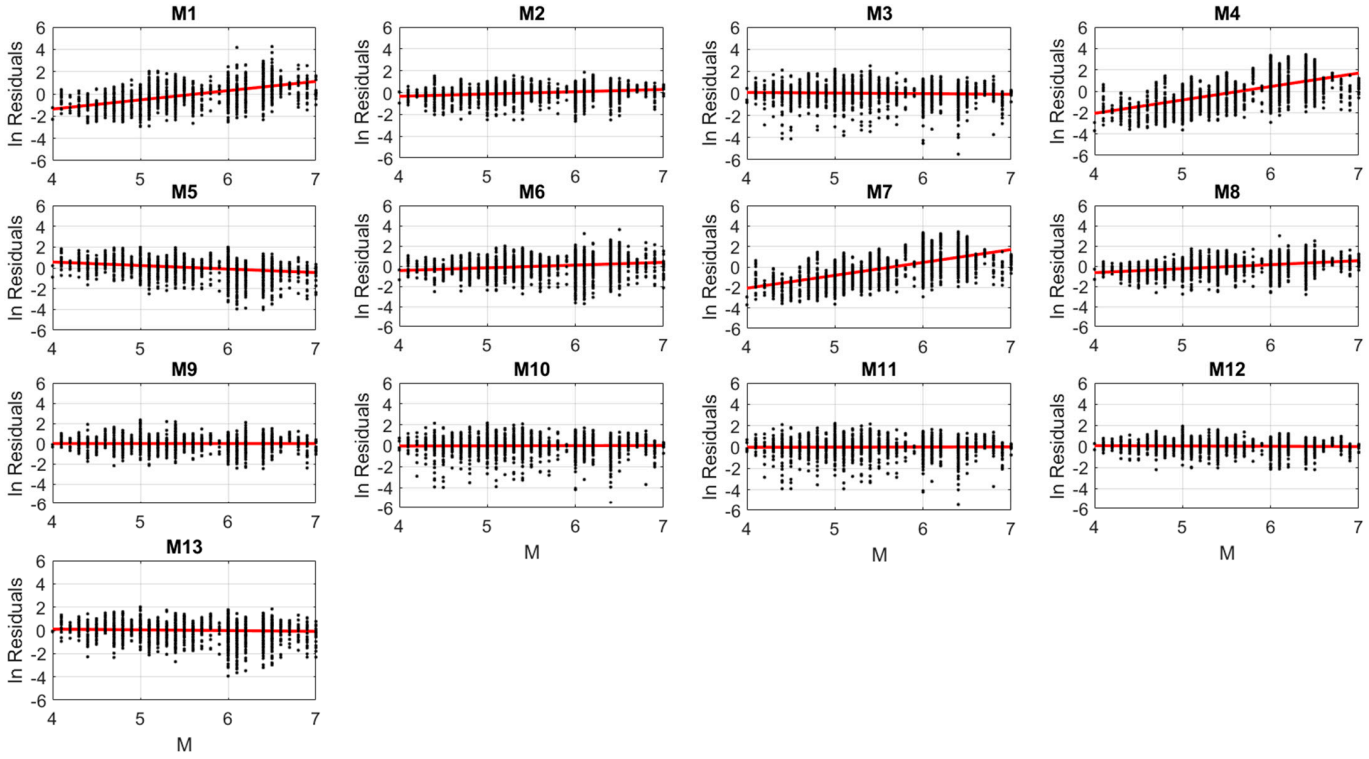


Figure 7. Residuals of nonlinear regression models with respect to the earthquake magnitude, M.

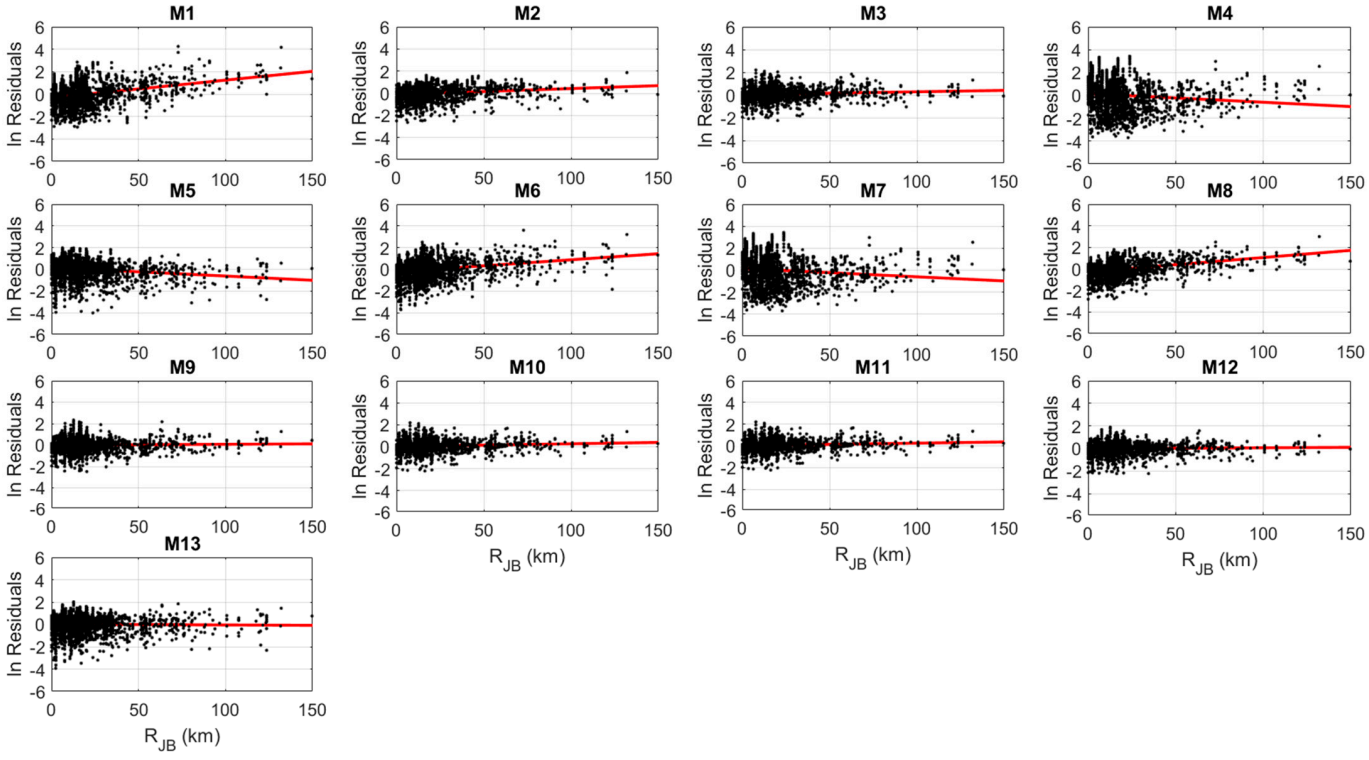


Figure 8. Residuals of nonlinear regression models with respect to the Joyner–Boore distance between the earthquake rupture and the recording station.

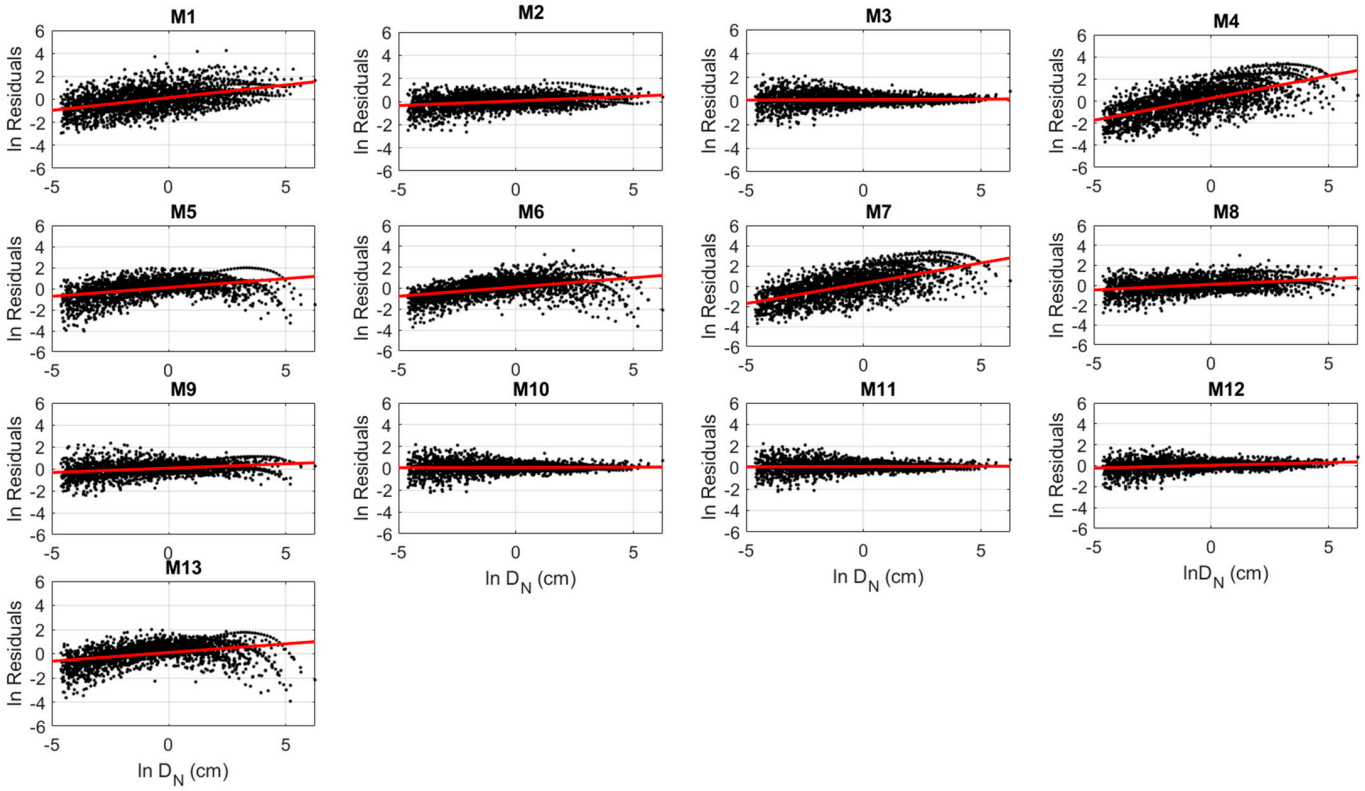


Figure 9. Residuals of nonlinear regression models with respect to the natural logarithm of the Newmark displacement.

Mixed-Effects Regression Based on the Residuals of Selected Models

The models for which the mixed-effects analysis was performed are M2, M3, M5, M9, M12 and M13. Those models represent the best performing models requiring one (M5, M13), two (M2, M9) and three (M3, M12) intensity measures, additionally to the critical acceleration. Figure 10 presents the between-event residuals (η) of the aforementioned models with respect to the earthquake magnitude (black squares). The red dots and the associated error bars denote the mean and standard deviation of these residuals within specific earthquake magnitude bins. Models M5 and M2 exhibit a linear trend, which decreases (M5) or increases (M2) with magnitude. However, when I_A in M5 is replaced by I_c to develop M13, the between-event residuals are reduced to zero, leading the aleatory variability of the model to be described solely by the within-event residuals. Models M9, M3 and M12 exhibit between-event residuals with no trend against earthquake magnitude and with a reduced associated standard deviation compared to models M5 and M2.

In Figure 11, the within-event residuals (ε) of the selected models are plotted against the source-to-site distance, R_{JB}. All selected models present no bias against R_{JB}. However, it is obvious that models M5 and M13 exhibit larger within-event standard deviation than the rest of the models. Moreover, Figure 12 presents ε against the V_{S30} of the recording stations, just to investigate any possible bias, which seems to be absent. Finally, Figure 13 presents the final aleatory variability as a function of the earthquake magnitude. The red curves indicate the between-event variability, which is expressed by the standard deviation of the between-event residuals (τ). The shape and final values of these curves have been chosen to fit the trend of τ with magnitude, which has been calculated within specific magnitude bins, and are shown as red squares. Similarly, the blue curves indicate the within-event variability, expressed by the standard deviation of the within-event residuals (φ). The black curves correspond to the total variability, which is calculated according to Equation (3).

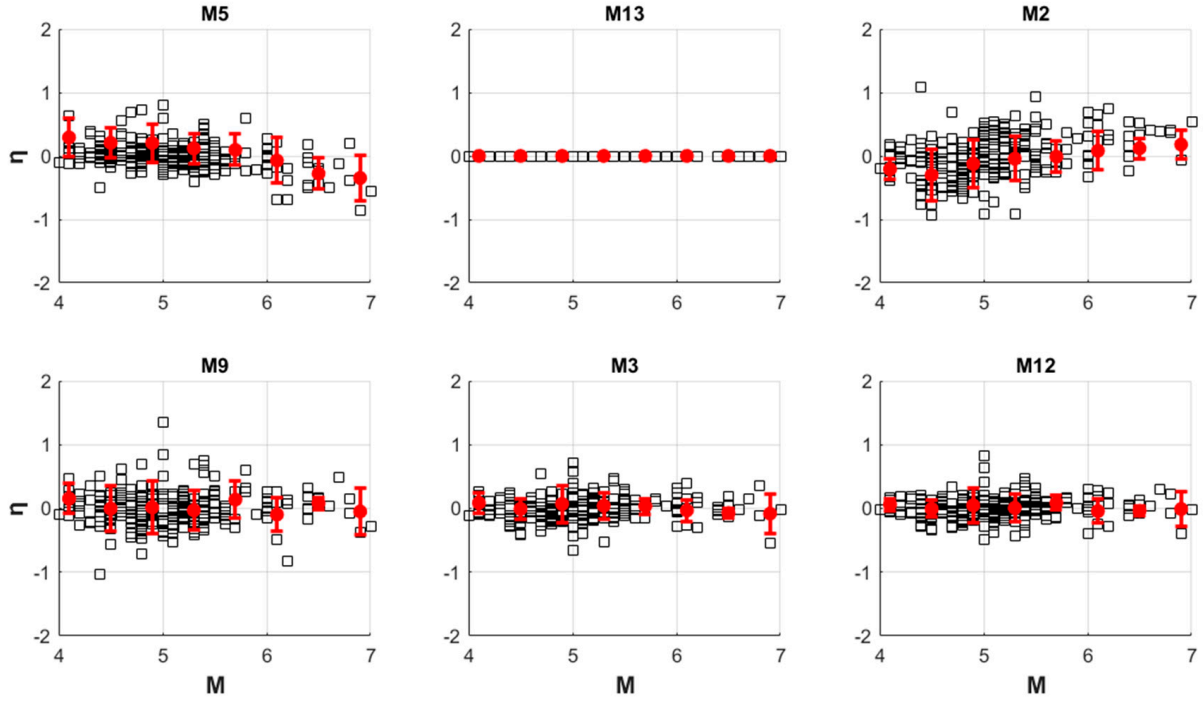


Figure 10. Between-event residuals for the selected nonlinear regression models with respect to the earthquake moment magnitude (M). The red dots and the associated error bars denote the mean and standard deviation of these residuals within specific earthquake magnitude bins.

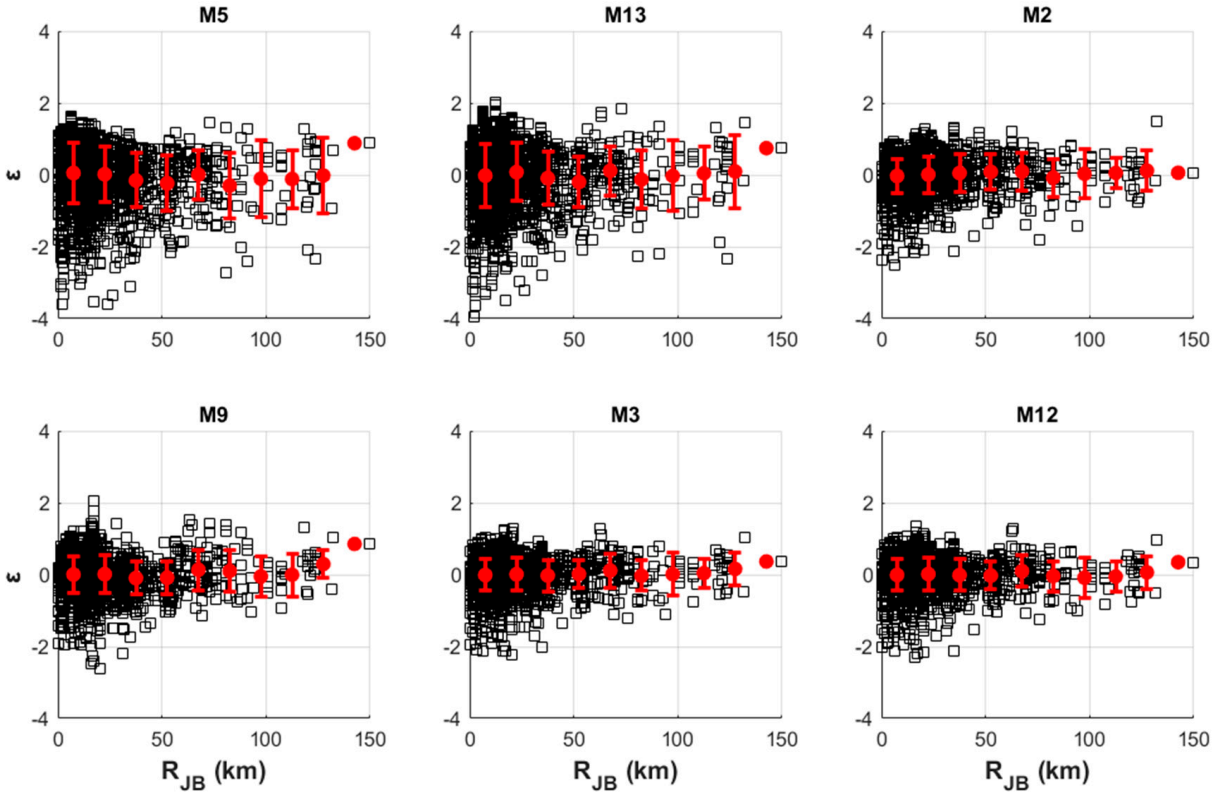


Figure 11. Within-event residuals for the selected nonlinear regression models with respect to the site-to-source distance R_{JB}. The red dots and the associated error bars denote the mean and standard deviation of these residuals within specific distance bins.

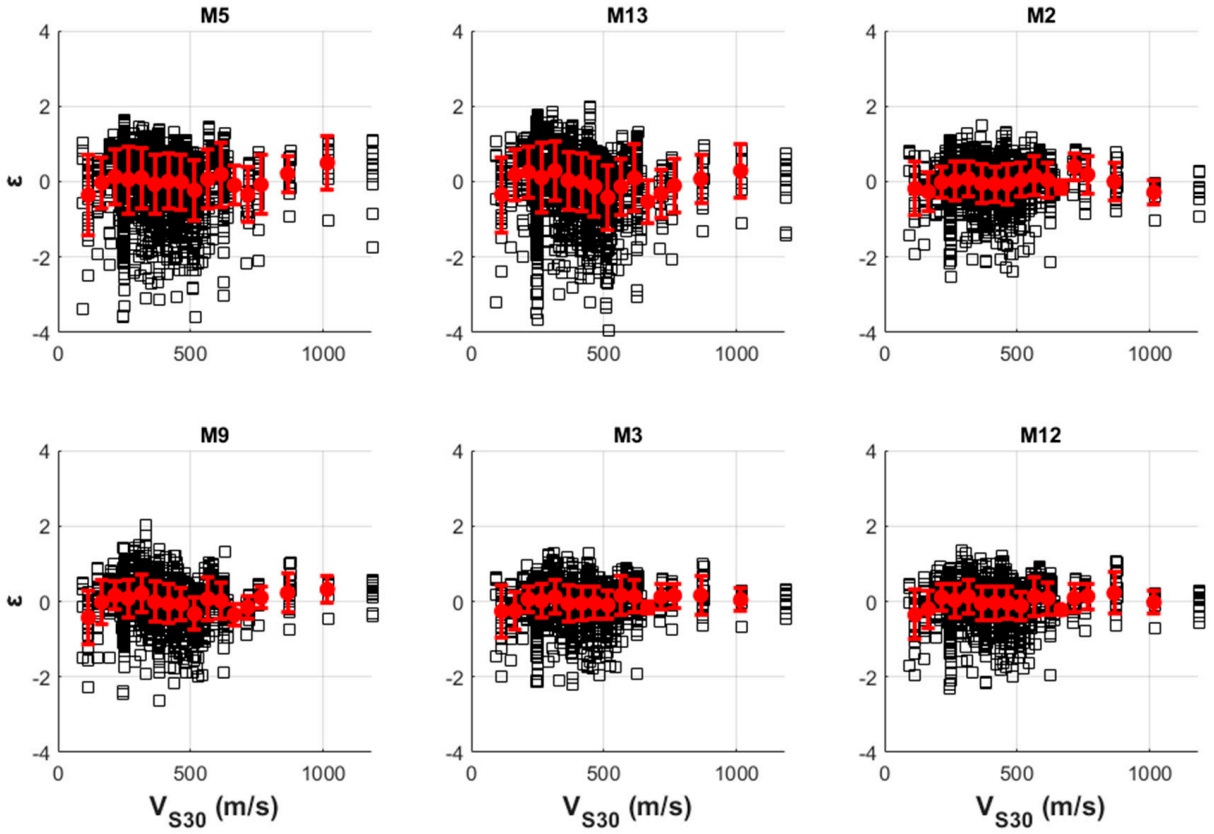


Figure 12. Within-event residuals for the selected nonlinear regression models with respect to V_{S30}. The red dots and the associated error bars denote the mean and standard deviation of these residuals within specific V_{S30} bins.

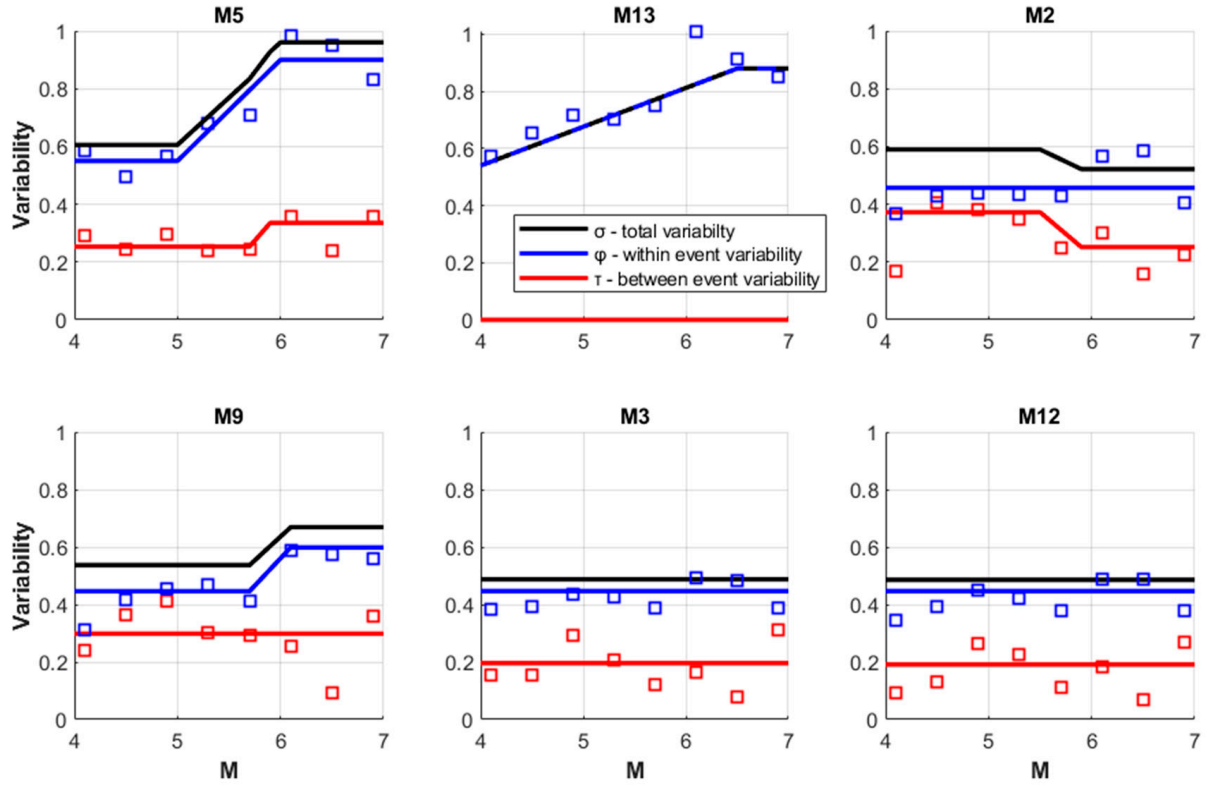


Figure 13. Between-, within- and total aleatory variability of the selected nonlinear regression models as a function of the earthquake magnitude.

Interestingly, Figure 13 shows that the shape of the aleatory variability functions are different for each nonlinear regression model. The best performing models, requesting three IMs and a_c, exhibit a constant aleatory variability with earthquake magnitude. Model M2, requesting *PGA*, *PGV* and a_c, presents a constant function for φ and a step-wise function for τ with a lower value for $M > 5.5$. Model M9, requesting *PGA*, I_c and a_c, depicts a constant function for τ and a step-wise function for φ with a lower value for M < 5.7. As explained above, model M13, incorporating only I_c and a_c, does not associate the residuals with the seismic events; hence, the total aleatory variability is described through φ, which increases linearly up to M6.5 and then attains its maximum value equal to 0.88. Model M5, which requires I_A and a_c, demonstrates a step-wise function for both τ and φ, with higher values for larger earthquake magnitudes. Table 4 presents the aleatory variability parameters of the selected nonlinear regression models in a tabulated form.

Table 4. Aleatory variability parameters of selected nonlinear regression models.

Model	τ	φ	σ
M5	0.253 for $4 \leq M \leq 5.7$ 0.336 for $M \geq 5.9$	0.55 for $4 \leq M \leq 5.0$ 0.9 for $M \geq 6.0$	0.605 for $4 \leq M \leq 5.0$ 0.96 for $M \geq 6.0$
M13	0	$-0.004 + 0.136 \times M$ for $4 \leq M \leq 6.5$ 0.88 for $M \geq 6.0$	$-0.004 + 0.136 \times M$ for $4 \leq M \leq 6.5$ 0.88 for $M \geq 6.5$
M2	0.372 for $4 \leq M \leq 5.5$ 0.252 for $M \geq 5.9$	0.457	0.590 for $4 \leq M \leq 5.5$ 0.522 for $M \geq 5.9$
M9	0.299	0.446 for $4 \leq M \leq 5.7$ 0.599 for $M \geq 6.1$	0.537 for $4 \leq M \leq 5.7$ 0.669 for $M \geq 6.1$
M3	0.196	0.447	0.488
M12	0.191	0.447	0.486

3.2. Shallow Artificial Neural Network Models

The ANN models were developed incorporating the predictor variables, which were used in models M3 and M12, shown in Table 2. As shown in Section 3.1, those two models were deemed the most effective in terms of uncertainty and the number of required inputs. Table 5 presents the standard deviation of the errors between the observations and the model predictions ($\sigma_{\ln DN}$), the R^2 coefficient, the AIC and the BIC, which can be considered performance indexes of the investigated ANN models for the prediction of Newmark displacement. The performance indexes of ANN3 and ANN12 have similar values, with the former exhibiting a slightly lower $\sigma_{\ln DN}$ and the latter presenting lower AIC and BIC values. A direct comparison between the capabilities of the nonlinear regression models (M3 and M12) and simple ANN models can be established by assessing the values of the performance indexes shown in Tables 3 and 4. Through this comparison, the ANN models seem to be slightly improved with respect to the nonlinear regression models, as they present lower $\sigma_{\ln DN}$ and BIC values, slightly higher R^2 coefficients and similar AIC values. The adequacy of the ANN models is also demonstrated in Figure 14, where the residuals between the observations and the predictions show no bias with respect to a_c, M, R_{JB} and ln D_N. Matlab function files are provided for the implementation of ANN3 and ANN12, as electronic supplements to this manuscript (see Supplementary Materials).

Table 5. Performance indexes of the investigated Artificial Neural Network Newmark displacement models.

ANN Model	ANN3				ANN12			
	Training	**Validation**	**Testing**	**All**	**Training**	**Validation**	**Testing**	**All**
$\sigma_{\ln DN}$	0.4554	0.4423	0.4599	0.4541	0.4391	0.4963	0.4967	0.4571
R^2	0.9579	0.9620	0.9520	0.9578	0.9615	0.9442	0.9499	0.9574
AIC	-	-	-	3272.2	-	-	-	3250.8
BIC	-	-	-	2926.0	-	-	-	2904.6
τ	-	-	-	0.149	-	-	-	0.153
φ	-	-	-	0.406	-	-	-	0.403
σ	-	-	-	0.432	-	-	-	0.431

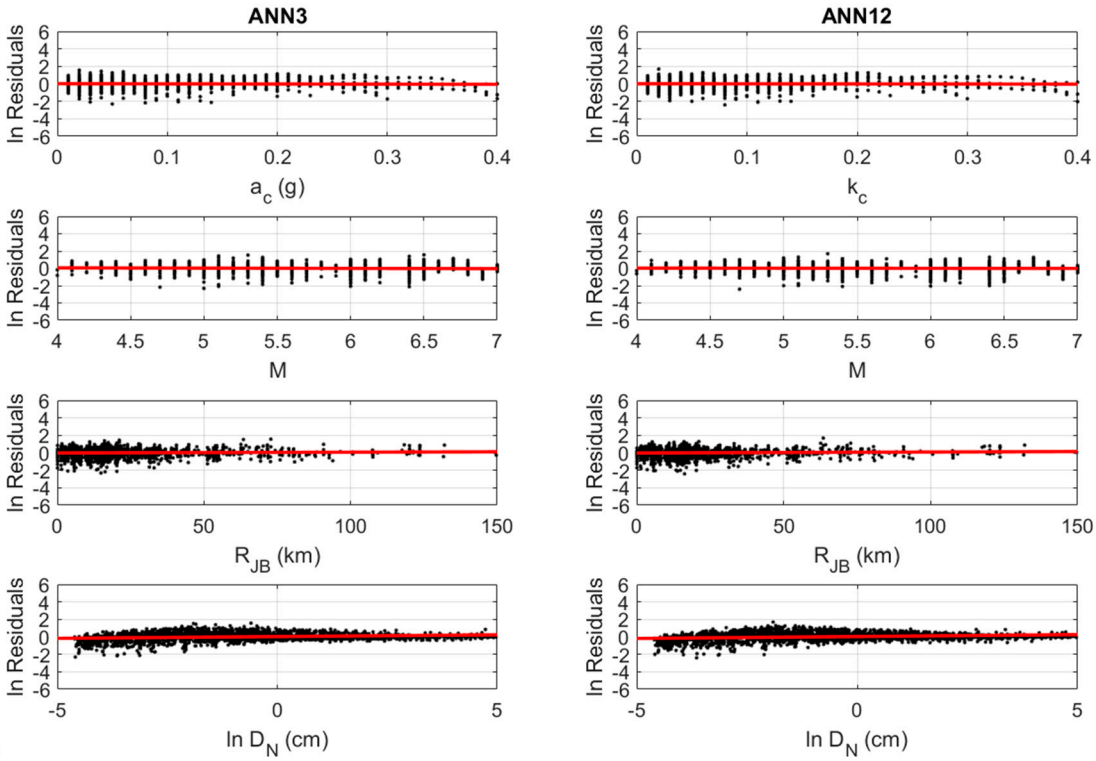
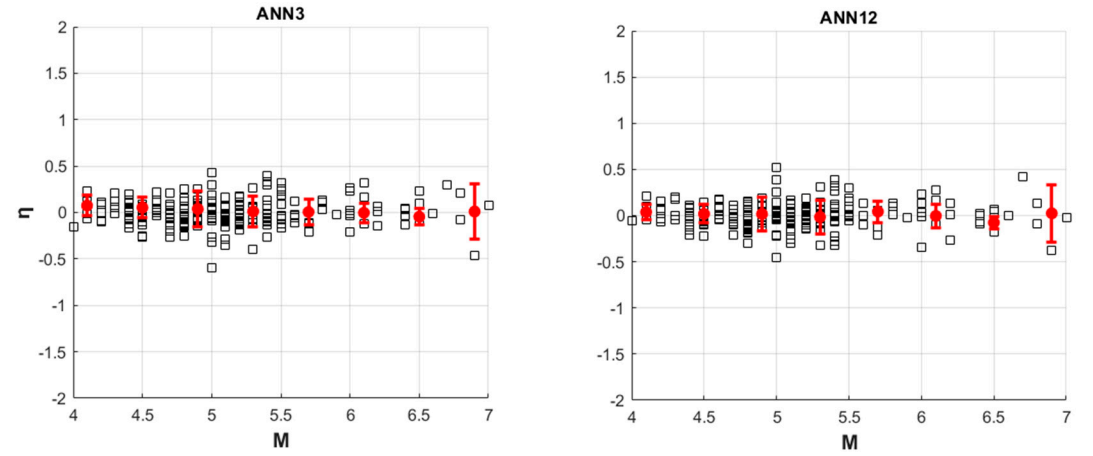


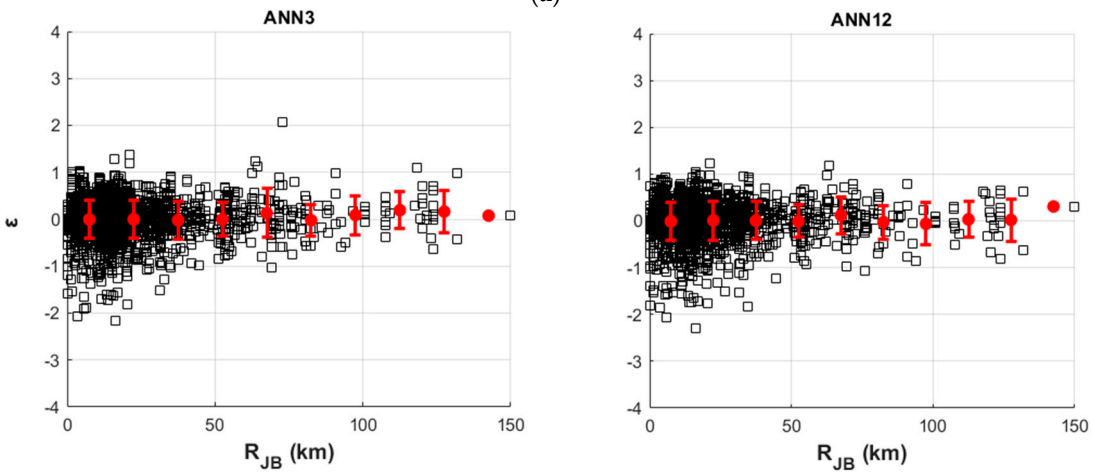
Figure 14. Residuals of ANN models with respect to the critical acceleration (a_c), the earthquake magnitude (M), the source-to-site distance (R_{JB}) and the natural logarithm of the Newmark displacement ($\ln D_N$).

Mixed-Effects Regression Based on the Residuals of ANN3 and ANN12

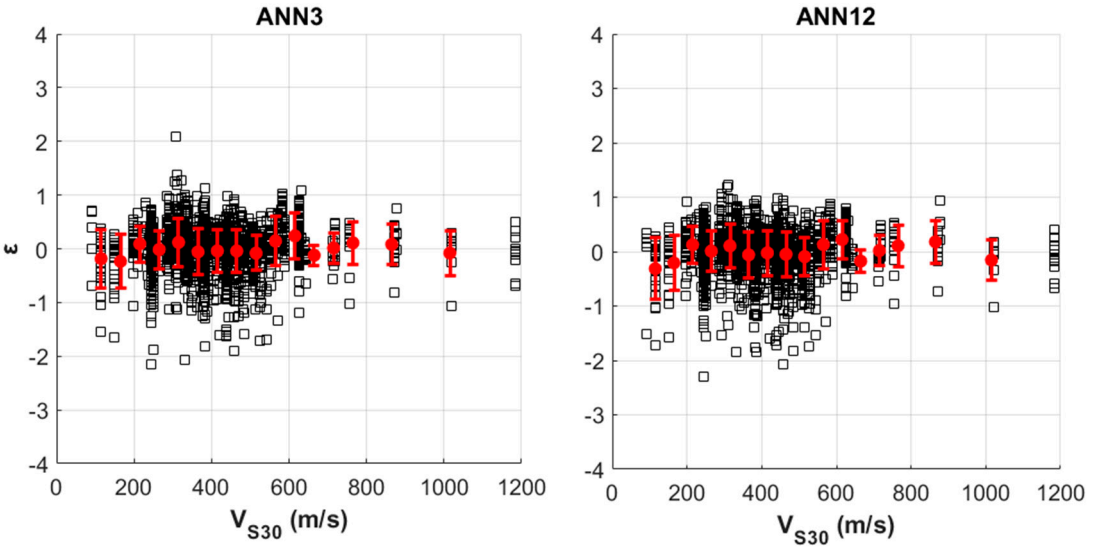
Following the same workflow to the nonlinear regression models, the uncertainty of the investigated ANN models was assessed through the mixed effects regression of their residuals (Figure 15). Figure 15a–c show that the between- and within-event residuals have a nearly zero mean value, limited standard deviation and no bias with respect to the earthquake magnitude, source-to-site distance and V_{S30}, which is quite similar to what was observed for the nonlinear regression models M3 and M12. However, Figure 15d, in conjunction with Figure 13, indicates that the ANN models show reduced total variability with respect to their nonlinear regression counterparts by 11%. This reduction is mostly attributed to a significantly smaller between-event variability by 20 to 24% and to a less important fall of the within-event variability by 9 to 10%. The tabulated values of the aleatory variability parameters of the ANN models are included in Table 5.



(**a**)



(**b**)



(**c**)

Figure 15. *Cont.*

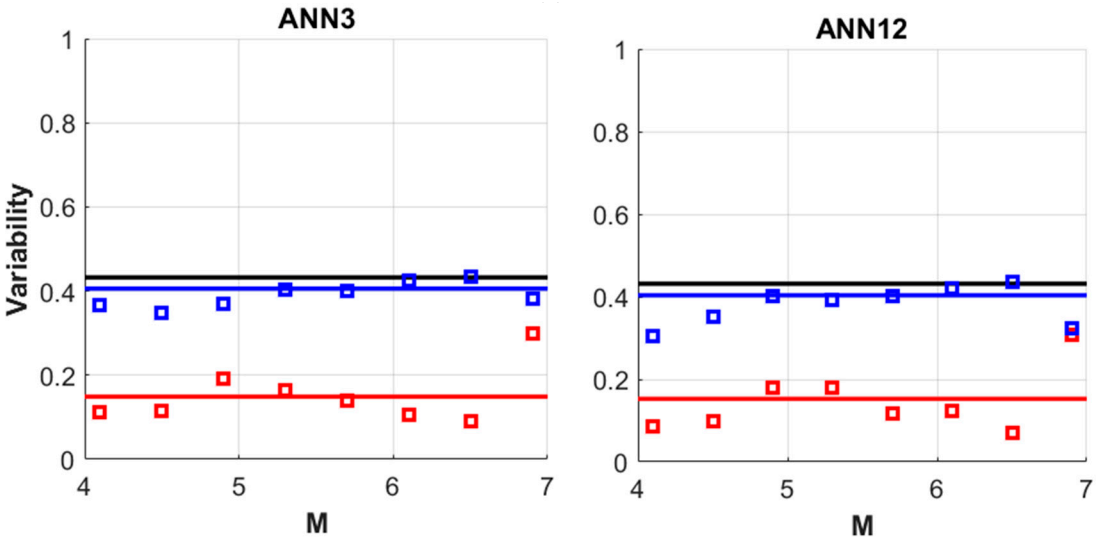


Figure 15. (**a**) Between-event residuals for the ANN models with respect to earthquake moment magnitude (M), (**b**) within-event residuals for the ANN models with respect to R_{JB}, (**c**) within-event residuals for the ANN models with respect to V_{S30} and (**d**) between-event, within-event and total aleatory variability of the selected ANN models as a function of the earthquake magnitude. The red dots and the associated error bars in (a), (b) and (c) denote the mean and standard deviation of these residuals within specific earthquake magnitude, distance and V_{S30} bins, respectively.

3.3. Comparison between Proposed and Existing Models

In this section, the comparison between the proposed Newmark displacement models and existing models found in the literature is undertaken. For this purpose, prediction models developed by Ambraseys and Menu (1988) [11], Jibson (2007) [14], Saygili and Rathje (2008) [15] and Chousianitis et al. (2014) [16] have been considered. The prediction of Newmark displacement using the existing models employs different ground motion parameters, such as *PGA*, *PGV* and I_A. The comparison between the mean predictions of the proposed and the existing models is performed for various combinations of earthquake magnitude (M_w), V_{S30} and a_c values in Figure 16. Mean *PGA*, *PGV* and I_A values are estimated from GMPEs, for which predictive adequacy has been evaluated against strong motion data from Greece, as shown in [33,34]. Therefore, the GMPEs of Boore et al. (2021) [27], Kotha et al. (2020) [35] and Chiou and Youngs (2014) [36], with their respective weights being the ones computed by [32], have been considered for the mean estimates of *PGA* and *PGV*, whereas the models of Huang et al. (2020) [37], Chousianitis et al. (2014) [16] and Bahrampouri et al. (2021) [38] have been utilized for the mean prediction of I_A. The proposed models, which include I_c as a predictive variable (M9, M12, M13), are not included in this section, as no predictive model has been found in the literature regarding this strong motion parameter. For the following calculation, normal fault rupture has been assumed for the calculation of the ground motion parameters.

Figure 16 shows that the trend of the proposed models' estimates is consistent with existing models. For a given M_w and V_{S30}, the slope displacement decreases with an increase in a_c and R_{JB}, whereas larger D_N values are observed for the M7.0 earthquake than M6.0. Models that include the (a_c/PGA) parameter present a cut-off distance beyond which no permanent displacements occur due to the *PGA* being lower than a_c. For the M6.0 earthquake, the majority of the proposed models (M2, M3, ANN3) provide similar mean predictions, whereas the M5 model deviates significantly beyond a 3 km distance. The deviation is mostly attributed to the functional form of M5, which includes only I_A and a_c. The predictions of M5 resemble to those of CH14, which is a model based on Greek strong motion data and utilizes a similar functional form. For the M7.0 earthquake, the differences among the mean predictions of the proposed models are highlighted. However, the differ-

ences are quite large between the existing models, as well. As shown in Figure 2, few data are available for M7.0 events in small distances. Hence, the deviations between the models developed using the current dataset may be attributed to the lack of sufficient data in the large magnitude–small distance region of the strong motion dataset. However, the model M3 is in very good agreement with the SR08c, which uses the same predictor variables as M3. The fact that SR08c has been calibrated to a worldwide dataset, which includes more data of large magnitude earthquakes at short distances, increases the confidence of the M3 predictions at short distances.

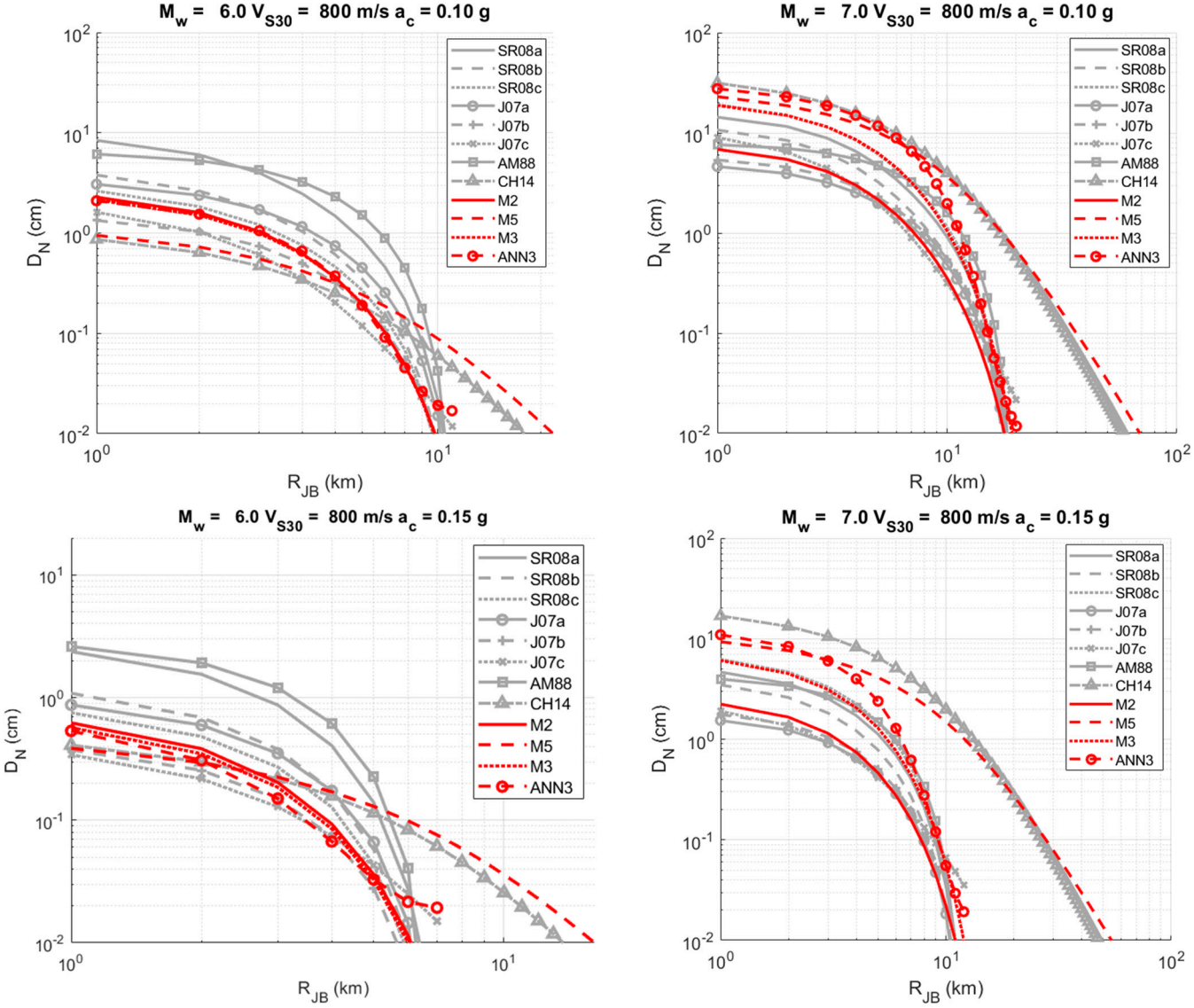


Figure 16. Comparison between the predictions of proposed Newmark displacement models (M2, M3, M5, ANN3) and existing models found in the literature (Note: SR08a, SR08b, SR08c—Saygili and Rathje, 2008 [15] with one, two and three intensity measures, respectively; J07a, J07b, J07—Jibson, 2007 [14] utilizing the a_c/PGA ratio, the a_c/PGA ratio and Mw and I_A and a_c, respectively; AM88: Ambraseys and Menu, 1988 [11]; CH14—Chousianitis et al., 2014 [16]).

In the next step, a comparative study, in terms of total variability ($\sigma_{\ln D}$), is performed between the proposed and the existing models. Table 6 presents the $\sigma_{\ln D}$ of the existing and the proposed models. It should be noted that the total variability reported in Figures 13 and 15d for the regression-based and ANN models, respectively, has been considered. Models M2, M3 and ANN3 present reduced aleatory variability with respect to

most of the existing models. The models SR08b and SR08c describe an increasing $\sigma_{\ln D}$ with a_c/PGA, and hence, the range of $\sigma_{\ln D}$ is reported in Table 6. Model M2 includes the same parameters as SR08b and exhibits reduced aleatory variability compared to the average $\sigma_{\ln D}$ of SR08b. Furthermore, models M3 and ANN3, which include the same parameters as SR08c, present average lower $\sigma_{\ln D}$ values than the SR08c.

Table 6. Aleatory variability ($\sigma_{\ln D}$) of existing and proposed Newmark displacement models.

Model	$\sigma_{\ln D}$
AM88	0.829
J07a	1.174
J07b	1.045
J07c	1.418
SR08a	1.13
SR08b	0.441–0.93
SR08c	0.24–0.99
CH14	0.532
M2	0.522–0.589
M3	0.488
M5	0.605–0.961
ANN3	0.432

3.4. Probabilistic Landslide Hazard Assessment

The framework of the probabilistic assessment of seismic-induced slope displacements, to demonstrate the effect of each Newmark displacement model on the sliding displacement hazard curve, was described in Section 2.3. More specifically, one-, two and three-IM Newmark displacement models are investigated, namely M5, M2, M3 and ANN3. The ground motion intensity is described through I_A in model M5 (one-IM model), through *PGA* and *PGV* in model M2 (two-IMs model) and through *PGA*, *PGV* and I_A in models M3 and ANN3 (three-IMs models).

As an illustrative example, we present here the probabilistic assessment of seismic-induced slope displacements for the cut slopes of a vertical road axis at a region located in Northern Greece, utilizing published data regarding the engineering properties of the local geological formations [31] and the seismic hazard assessment for *PGA* and *PGV* [32] and I_A [33]. With reference to Equations (1)–(5), *PGA* is considered as *IM*1, *PGV* is considered as *IM2* and I_A is considered as *IM3*. Therefore, for the implementation of model M5, as a one-IM model, the hazard curve of I_A for the investigated site is necessary, whereas for the implementation of M2, M3 and ANN3, the hazard curve of *PGA* is needed, as well as the M–R seismic hazard disaggregation (Figure 4). Furthermore, the GMPE, which is used for the calculation of *PGA* and *PGV*, is the one proposed by [27], which is the most updated for Greece, whereas the GMPE of [37] is used for the estimation of I_A, as it has been proven to be appropriate for use in Greece [34].

Figure 17 presents the results of the probabilistic assessment of seismic-induced slope displacements, which was performed for four values of critical acceleration, according to the methodology described above. Significant differences are observed among the resulting slope displacement hazard curves originating from the implementation of different Newmark displacement models, especially for low a_c values, where relatively large displacements are anticipated. The proposed models, which include three IMs (M3 and ANN3), predict much larger displacement levels than models M5 and M2, which include one and two IMs, respectively. As the critical acceleration increases, and hence the displacements are reduced, the differences among the hazard curves are diminishing. The quantitative

differences arising from the implementation of different Newmark displacement models are presented using some examples. More specifically, we consider three design levels, one with a return period of 475 years (λ_D = 0.0021 yr^{-1}), one with a return period of 1000 years (λ_D = 0.001 yr^{-1}) and one with a return period of 2500 years (λ_D = 0.0004 yr^{-1}). The estimated displacements for these design levels, as retrieved from the hazard curves of Figure 17, are given in Table 7. Each cell of the table is colored according to the thresholds of Jibson and Michael (2009) [39], which qualitatively characterize the severity of the landslide hazard. The values for a_c equal to 0.3 g are omitted, as insignificant displacements are predicted for the considered design levels.

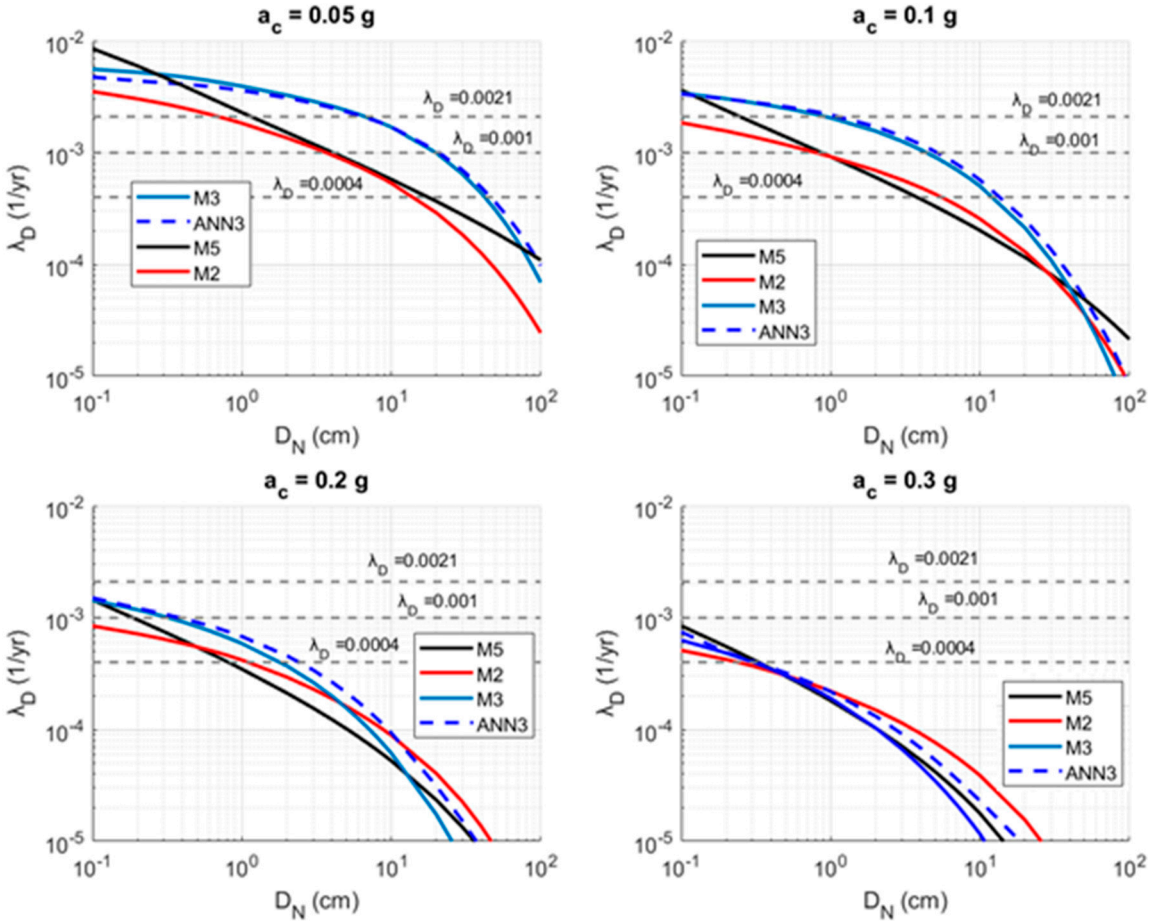


Figure 17. Results of probabilistic assessment of seismic-induced slope displacements for various critical acceleration values for Komotini, Greece.

Table 7. Newmark displacement estimates (in cm) for three design levels and critical acceleration values.

Hazard Level (Jibson and Michael, 2009) [39]:					**Low**		**Moderate**		**High**		**Very High**	
	a_c = 0.05 g				**a_c = 0.1 g**				**a_c = 0.2 g**			
λ_D	M5	M2	M3	ANN3	M5	M2	M3	ANN3	M5	M2	M3	ANN3
0.0021	1.25	0.7	6.73	6.5	0.26	0	0.93	1.19	0	0	0	0
0.001	4.08	3.71	19.96	21.32	0.87	0.8	4.44	5.18	0.19	0	0.33	0.39
0.0004	20	15.42	40	46.92	3.875	5.60	13.45	15.31	0.8	1.15	1.86	2.5

Models M5 and M2, although they use one and two IMs, respectively, to describe the ground motion, they provide similar Newmark displacement estimates, for almost all

the design levels. However, models M3 and ANN3, which describe the ground motion through three intensity measures and present lower standard errors, provide significantly larger D_N estimates for the considered cases with low a_c (0.05 and 0.1 g) and design levels. The correlation of D_N with three IMs leads to more accurate estimates, as shown by the lower model variability compared to when two or one IM is used (Table 6). Therefore, the differences shown above pose a strong indication that multiple IMs should be incorporated for a more precise assessment of the seismic hazard at a site or a region.

4. Discussion

The present study uses the most updated strong motion dataset for Greece to develop and propose regional Newmark displacement models, which incorporate multiple intensity measures of ground motion and various functional forms. The proposed models were produced through nonlinear regression; however, the Artificial Neural Network algorithm was implemented, as well, to highlight its capabilities of simulating strong nonlinearities between the ground motion parameters and the Newmark displacements. Models that include three intensity measures (PGA, PGV and I_A or I_c) were deemed superior to models that include one or two, exhibiting significantly lower standard errors. This is in agreement with other studies in the literature [14,20,22,23]. Interestingly, the inclusion of the characteristic intensity, I_c, instead of I_A led to a reduction in the standard error. Nevertheless, this parameter has not gained the appropriate attention from the scientific community, as, to the authors' knowledge, no empirical model exists (GMPE) that correlates its prediction with the earthquake rupture and site properties (M, R, V_{S30}). Therefore, the inclusion of Newmark displacement models that incorporate I_c in a probabilistic framework for the assessment of seismic-induced slope displacements is difficult. A future step forward would be the development of global or regional empirical models for I_c, based on strong motion data.

The trends in the mean estimates of the proposed models agree with the ones of existing models that have been calibrated based on worldwide or regional data. Moreover, the proposed modes are improved compared to the latest Newmark displacement modeled for Greece, as they exhibit reduced uncertainty in their predictions. Nevertheless, it should be noted that the applicability of the proposed models is defined by the range of values covered by the strong motion dataset. Furthermore, in this study, several Newmark displacement models are proposed, which describe the ground motion at various levels of accuracy, incorporating one, two or three ground motion parameters. Therefore, they pose a significant contribution to the assessment of seismic-induced slope displacements for Greece and therefore to the sustainability of the communities, especially in mountainous regions. In such a region in Greece, the probabilistic assessment of seismic-induced slope displacements was undertaken, implementing the Newmark displacement modes, which were proposed. The effect of the selection of the Newmark displacement model on the slope displacement hazard curves is significant, with the models correlating the Newmark displacement with three IMs providing larger hazard levels compared to the ones that use one or two IMs. This stands for the specific site presented herein and should not be expected in every situation. It is the authors' belief that the seismogenic environment of the site under investigation affects the resulting seismic hazard curves in terms of various intensity measures (PGA, PGV, I_A), as well as the corresponding seismic slope displacement hazard curve. A means to address the epistemic uncertainty associated with the prediction of slope displacements would be to combine multiple Newmark displacement models through the logic-tree approach with weights linked to their predictive accuracy. The regional implementation of the probabilistic assessment of seismic-induced slope displacements in mountainous areas, using appropriate empirical models for the region at interest, is a step forward towards the detection of vulnerable sites, which leads to the design of prioritization schemes for mitigation measures and, ultimately, to an improvement in the social and environmental sustainability.

Supplementary Materials: The following supporting information can be downloaded at: https://www.mdpi.com/article/10.3390/su16062240/s1, ANN3.m: MATLAB function for implementation of the ANN3 model; ANN12.m: MATLAB function for implementation of the ANN12 model.

Author Contributions: Conceptualization, D.S. and N.K.; methodology, D.S.; software, D.S.; investigation, D.S.; resources, I.M.D.; writing—original draft preparation, D.S.; writing—review and editing, N.K. and I.M.D.; supervision, N.K.; project administration, I.M.D. All authors have read and agreed to the published version of the manuscript.

Funding: We acknowledge the support of this work by the project "Risk and Resilience Assessment Center–Prefecture of East Macedonia and Thrace-Greece" (MIS 5047293), which is implemented under the Action "Reinforcement of the Research and Innovation Infrastructure", funded by the Operational Program "Competitiveness, Entrepreneurship and Innovation" (NSRF 2014–2020), and co-financed by Greece and the European Union (European Regional Development Fund).

Institutional Review Board Statement: Not applicable.

Informed Consent Statement: Not applicable.

Data Availability Statement: No new data were created or analyzed in this study. Data sharing is not applicable to this article.

Conflicts of Interest: The authors declare no conflicts of interest.

References

1. Newmark, N.M. Effects of earthquakes on dams and embankments. *Geotechnique* **1965**, *15*, 849–867. [CrossRef]
2. Rathje, E.M.; Antonakos, G. A unified model for predicting earthquake-induced sliding displacements of rigid and flexible slopes. *Eng. Geol.* **2011**, *122*, 51–60. [CrossRef]
3. Cui, Y.; Liu, A.; Xu, C.; Zheng, J. A modified Newmark method for calculating permanent displacement of seismic slope considering dynamic critical acceleration. *Adv. Civ. Eng.* **2019**, *2019*, 9782515. [CrossRef]
4. Ji, J.; Wang, W.; Cui, Z.; Li, Y.; Song, J.; Gao, Y. A simplified nonlinear coupled Newmark displacement model with degrading yield acceleration for seismic slope stability analysis. *Int. J. Numer. Anal. Methods Geomech.* **2021**, *45*, 1303–1322. [CrossRef]
5. Keefer, D.K. Landslides caused by earthquakes. *GSA Bull.* **1984**, *95*, 406–421. [CrossRef]
6. Seed, H.B.; Martin, G.R. The seismic coefficient in earth dam design. *J. Soil Mech. Found. Div.* **1966**, *92*, 25–58. [CrossRef]
7. Makdisi, F.I.; Seed, H.B. Simplified procedure for estimating dam and embankment earthquake induced deformations. *J. Geotech. Eng. Div.* **1978**, *104*, 849–867. [CrossRef]
8. Bray, J.D.; Rathje, E.M. Earthquake-induced displacements of solid-waste landfills. *J. Geotech. Geoenvironmental Eng.* **1998**, *124*, 242–253. [CrossRef]
9. Rathje, E.M.; Bray, J.D. An examination of simplified earthquake-induced displacement procedures for earth structures. *Can. Geotech. J.* **1999**, *36*, 72–87. [CrossRef]
10. Rathje, E.M.; Bray, J.D. Nonlinear coupled seismic sliding analysis of earth structures. *J. Geotech. Geoenvironmental Eng.* **2000**, *126*, 1002–2014. [CrossRef]
11. Ambraseys, N.N.; Menu, J.M. Earthquake-induced ground displacements. *Earthq. Eng. Struct. Dyn.* **1988**, *16*, 985–1006. [CrossRef]
12. Bray, J.D.; Augello, A.J.; Leonards, G.A.; Repetto, P.C.; Byrne, R.J. Seismic stability procedures for solid-waste landfills. *J. Geotech. Eng.-ASCE* **1995**, *121*, 139–151. [CrossRef]
13. Bray, J.D.; Travasarou, T. Simplified procedure for estimating earthquake-induced deviatoric slope displacements. *J. Geotech. Geoenvironmental Eng.* **2007**, *133*, 381–392. [CrossRef]
14. Jibson, R.W. Regression models for estimating coseismic landslide displacement. *Eng. Geol.* **2007**, *91*, 209–218. [CrossRef]
15. Saygili, G.; Rathje, E. Empirical Predictive Models for Earthquake-Induced Sliding Displacements of Slopes. *J. Geotech. Geoenvironmental Eng.* **2008**, *134*, 790–803. [CrossRef]
16. Chousianitis, K.; Del Gaudio, V.; Kalogeras, I.; Ganas, A. Predictive model of Arias intensity and Newmark displacement for regional scale evaluation of earthquake-induced landslide hazard in Greece. *Soil Dyn. Earthq. Eng.* **2014**, *65*, 11–29. [CrossRef]
17. Du, W.; Wang, G. A one-step Newmark displacement model for probabilistic seismic slope displacement hazard analysis. *Eng. Geol.* **2016**, *205*, 12–23. [CrossRef]
18. Tsai, C.; Chien, Y. A general model for predicting the earthquake-induced displacements of shallow and deep slope failures. *Eng. Geol.* **2016**, *206*, 50–59. [CrossRef]
19. Zhang, Y.B.; Xiang, C.L.; Chen, Y.L.; Cheng, Q.G.; Xiao, L.; Yu, P.C.; Chang, Z.W. Permanent displacement models of earthquake-induced landslides considering near-fault pulse-like ground motions. *J. Mt. Sci.* **2019**, *16*, 1244–1257. [CrossRef]
20. Wang, M.X.; Huang, D.R.; Wang, G.; Li, D.Q. SS-XGBoost: A machine learning framework for predicting newmark sliding displacements of slopes. *J. Geotech. Geoenvironmental Eng.-ASCE* **2020**, *146*, 04020074. [CrossRef]
21. Gade, M.; Nayek, P.S.; Dhanya, J. A new neural network-based prediction model for Newmark's sliding displacements. *Bull. Eng. Geol. Environ.* **2021**, *80*, 385–397. [CrossRef]

22. Cheng, Y.; Wang, J.; He, Y. Prediction Models of Newmark Sliding Displacement of Slopes Using Deep Neural Network and Mixed-effect Regression. *Comput. Geotech.* **2023**, *156*, 105264. [CrossRef]
23. Nayek, P.S.; Gade, M. Artificial neural network-based fully data-driven models for prediction of newmark sliding displacement of slopes. *Neural Comput. Appl.* **2022**, *34*, 9191–9203. [CrossRef]
24. Macedo, J.; Bray, J.; Abrahamson, N.; Travasarou, T. Performance-Based Probabilistic Seismic Slope Displacement Procedure. *Earthq. Spectra* **2018**, *34*, 673–695. [CrossRef]
25. Rathje, E.M.; Saygili, G. Probabilistic assessment of earthquake-induced sliding displacements of natural slopes. *Bull. N. Z. Soc. Earthq. Eng.* **2009**, *42*, 18–27. [CrossRef]
26. Margaris, B.; Scordilis, E.M.; Stewart, J.P.; Boore, D.M.; Theodoulidis, N.; Kalogeras, I.; Melis, N.S.; Skarlatoudis, A.A.; Klimis, N.; Seyhan, E. Hellenic Strong-Motion Database with Uniformly Assigned Source and Site Metadata for the Period 1972–2015. *Seismol. Res. Lett.* **2021**, *92*, 2065–2080. [CrossRef]
27. Boore, D.; Stewart, J.P.; Skarlatoudis, A.; Seyhan, E.; Margaris, B.; Theodoulidis, N.; Scordilis, E.; Kalogeras, I.; Klimis, N.; Melis, N. A Ground-Motion Prediction Model for Shallow Crustal Earthquakes in Greece. *Bull. Seismol. Soc. Am.* **2021**, *111*, 857–874. [CrossRef]
28. Marquardt, D. An Algorithm for Least-Squares Estimation of Nonlinear Parameters. *SIAM J. Appl. Math.* **1963**, *11*, 431–441. Available online: https://www.jstor.org/stable/2098941 (accessed on 20 November 2023). [CrossRef]
29. Abrahamson, N.A.; Youngs, R.R. A stable algorithm for regression analyses using the random effects model. *Bull. Seismol. Soc. Am.* **1992**, *82*, 505–510. [CrossRef]
30. Bazzurro, P.; Cornell, C.A. Disaggregation of seismic hazard. *Bull. Seismol. Soc. Am.* **1999**, *89*, 501–520. [CrossRef]
31. Sotiriadis, D.; Klimis, N.; Margaris, B.; Koutsoupaki, E.I.; Petala, E.; Dokas, I. Probabilistic Seismic Risk Analysis of Urban Road Networks in Mountainous areas. In *The Challenges of Disaster Planning, Management and Resilience*; Michail, C., Ed.; Nova Science Publishers, Inc.: New York, NY, USA, 2023; Chapter 6; pp. 75–100. [CrossRef]
32. Sotiriadis, D.; Margaris, B.; Klimis, N.; Dokas, I.M. Seismic Hazard in Greece: A Comparative Study for the Region of East Macedonia and Thrace. *GeoHazards* **2023**, *4*, 239–266. [CrossRef]
33. Sotiriadis, D.; Margaris, B.; Klimis, N. Evaluation of ground motion models for Arias Intensity (IA), Cumulative Absolute Velocity (CAV) and significant duration for Greece and preliminary PSHA results. In Proceedings of the 3rd International Conference on Natural Hazards & Infrastructure, Athens, Greece, 5–7 July 2022.
34. Sotiriadis, D.; Margaris, B. Evaluation of the predictive performance of regional and global ground motion predictive equations against Greek strong motion data. *Soil Dyn. Earthq. Eng.* **2023**, *165*, 107656. [CrossRef]
35. Kotha, S.R.; Weatherill, G.; Bindi, D.; Cotton, F. A regionally-adaptable ground-motion model for shallow crustal earthquakes in Europe. *Bull. Earthq. Eng.* **2020**, *18*, 4091–4125. [CrossRef]
36. Chiou, B.S.-J.; Youngs, R.R. Update of the Chiou and Youngs NGA model for the average horizontal component of peak ground motion and response spectra. *Earthq. Spectra* **2014**, *30*, 1117–1153. [CrossRef]
37. Huang, C.; Tarbali, K.; Galasso, C. Correlation properties of integral ground-motion intensity measures from Italian strong-motion records. *Earthq. Eng. Struct. Dyn.* **2020**, *49*, 1581–1598. [CrossRef]
38. Bahrampouri, M.; Rodriguez-Marek, A.; Green, R.A. Ground motion prediction equations for Arias Intensity using the Kik-net database. *Earthq. Spectra* **2021**, *37*, 428–448. [CrossRef]
39. Jibson, R.W.; Michael, J.A. *Maps Showing Seismic Landslide Hazards in Anchorage, Alaska*; US Geological Survey Reston: Reston, VA, USA, 2009. [CrossRef]

Disclaimer/Publisher's Note: The statements, opinions and data contained in all publications are solely those of the individual author(s) and contributor(s) and not of MDPI and/or the editor(s). MDPI and/or the editor(s) disclaim responsibility for any injury to people or property resulting from any ideas, methods, instructions or products referred to in the content.